Chem Soc Rev

Methane Activation by ZSM-5-supported Transition Metal Centers

Journal:	*Chemical Society Reviews*
Manuscript ID	CS-REV-08-2020-001016.R2
Article Type:	Review Article
Date Submitted by the Author:	06-Nov-2020
Complete List of Authors:	Kiani, Daniyal; Lehigh University, Department of Chemical & Biomolecular Engineering Sourav, Sagar; Lehigh University, Department of Chemical & Biomolecular Engineering Tang, Yadan; Cummins Inc Baltrusaitis, Jonas; Lehigh University, Department of Chemical & Biomolecular Engineering Wachs, Israel; Lehigh University, Department of Chemical & Biomolecular Engineering

Methane Activation by ZSM-5-supported Transition Metal Centers

Daniyal Kiani[$#], Sagar Sourav[$#], Yadan Tang[+] Jonas Baltrusaitis[#] and Israel E. Wachs[#*]

[#]Department of Chemical and Biomolecular Engineering, Lehigh University, Bethlehem, PA, 18015, USA

[+]Current address: Cummins, Inc. 1900 McKinley Avenue, Columbus, Indiana, 47201, USA

[$] DK and SS contributed equally.

* Corresponding author: iew0@lehigh.edu

Abstract.

This review focuses on recent fundamental insights about methane dehydroaromatization (MDA) to benzene over ZSM-5-supported transition metal oxide-based catalysts (MO_x/ZSM-5, where M= V, Cr, Mo, W, Re, Fe). Benzene is an important organic intermediate, used for the synthesis of chemicals like ethylbenzene, cumene, cyclohexane, nitrobenzene and alkylbenzene. Current production of benzene is primarily from crude oil processing, but due to the abundant availability of natural gas, there is much recent interest in developing direct processes to convert CH_4 to liquid chemicals. Among the various gas-to-liquid methods, the thermodynamically-limited Methane DehydroAromatization (MDA) to benzene under non-oxidative conditions appears very promising as it circumvents deep oxidation of CH_4 to CO_2 and does not require the use of a co-reactant. The findings from the MDA catalysis literature is critically analyzed with emphasis on *in situ* and *operando* spectroscopic characterization to understand the molecular level details regarding the catalytic sites before and during the MDA reaction. Specifically, this review discusses the anchoring sites of the supported MO_x species on the ZSM-5 support, molecular structures of the initial dispersed surface MO_x sites, nature of the active sites during MDA, reaction mechanisms, rate-determining step, kinetics and catalyst activity of the MDA reaction. Finally, suggestions are given regarding future experimental investigations to fill the information gaps currently found in the literature.

1. Introduction

The current abundance of natural gas (NG) across the globe, from recent discoveries of large shale gas deposits in North America and methane hydrates beneath permafrost or in shallow sediments along deep-water continental margins[1], is projected to persist in the coming years due to improvements in both exploration and extraction technologies.[1] Owing to the large surplus, NG is anticipated to serve as the primary energy resource in the transition period, as the global economies transition off oil-based energy generation to renewable energy-based economies of the future.[2] Currently, however, NG is either used as the fuel for power generation and transportation or simply flared to the atmosphere, owing to a deficiency of industrially feasible on-site conversion processes. In the past decades, various attempts have been made to convert methane (CH_4), the primary component (~ 70-90%) of NG, to value-added products. A schematic summary of the direct CH_4 conversion methods to produce olefins, aromatics and commodity chemicals is presented in **Figure 1.** Among these processes, literature reports on the following can be found: methane to methanol and formaldehyde via partial oxidation (POM)[2], (ii) methane to ethane and ethylene via oxidative coupling (OCM),[3–6] (iii) methane to benzene via non-oxidative methane dehydro-aromatization (MDA, also known as DHA) [7–9], (iv) methane to olefins, aromatics, and hydrogen (MTOAH)[10,11], and methane to halogenated derivates via methane oxy-halogenation.[12–14] Note that although there are various indirect processes to valorize CH_4 like the industrially employed syngas process, they are simply more capital intensive and exhibit a larger carbon footprint than potential direct conversion processes.[3,12,14] Given that a significant portion of the total NG is located in stranded locations, building large scale syngas plants remains unfeasible, leading to hundreds of billions of cubic meters of NG being flared from a lack of direct conversion methods.[15] In the past decade, policymakers have moved to reduce NG flaring practices across the globe by introducing

regulations and initiatives like the popular *Zero Routine Flaring by 2030* initiative,[16] further fueling the research on direct catalytic CH_4 valorization processes.

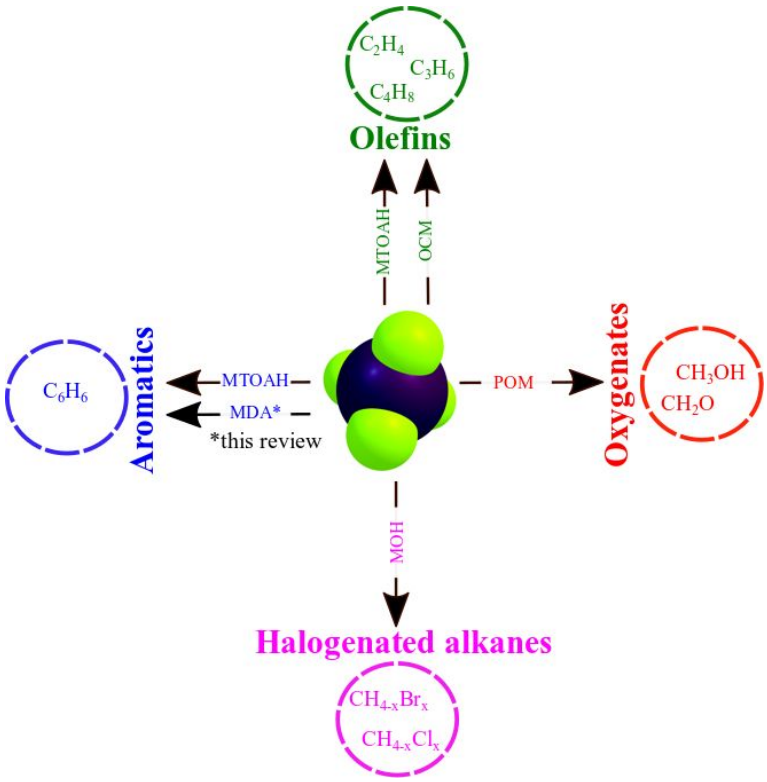

Figure 1. *Direct routes for CH_4 valorization.*

Metal oxides supported on ZSM-5 constitute an essential class of versatile catalysts that continues to receive both academic and industrial researchers' attention owing to the various reactions they catalyze.[7,17–29] For example, VO_x/ZSM-5 catalysts have been studied for selective catalytic reduction (SCR) of NO_x with NH_3[17], CrO_x/ZSM-5 catalysts are effective for oxidative dehydrogenation (ODH) of ethane to ethylene with CO_2[26], MoO_x/ZSM-5 have been investigated for non-oxidative methane dehydroaromatization (MDA) and partial oxidation of methane to formaldehyde[19], WO_x/ZSM-5 have been examined for methane oxidation and non-oxidative MDA[30,31], ReO_x/ZSM-5 have been studied for the conversion of ethane to benzene and MDA[24,29],

ZnO_x/ZSM-5 catalysts have been found to catalyze the aromatization of alkanes and alcohols[32], etc. This review focuses on a subset of the broader zeolite catalysis literature, i.e., ZSM-5-supported transition metal oxides (MO_x/ZSM-5) where M can be V, Cr, Mo, Re, W or Fe, specifically for MDA to produce benzene. Very recently, ZSM-5 supported group IX (CoO_x/ZSM-5)[33] and group X (NiO_x/ZSM-5)[34] catalysts have also been found to be active towards MDA reaction. However, they will not be covered in this review since presently little molecular-level information about these catalysts based on *in-situ* and *operando* characterization including Raman spectroscopy, X-ray absorption spectroscopy (XAS), etc is available.

MDA with supported MoO_x/ZSM-5 catalysts was first reported in 1993.[8] However, alkanes-to-benzene conversion using zeolite-based catalysts, in general, was actually pioneered in the period of 1974-1989 by a Russian group, which has largely been unrecognized.[35–37] Compared to other direct, oxidative processes, the non-oxidative environment for benzene production from methane sparked great interest due to its high product selectivity. This pioneering work, since then, has inspired investigations of other similar catalyst systems composed of group V-VII transition metal oxides supported on zeolite.[7] A few excellent reviews on methane dehydroaromatization (MDA) over zeolite supported transition metal oxide-based catalysts are available in literature[38–41] and the readers are directed to go over them to gain more insights on the following: (i) development of various conventional (Mo-oxide based catalysts) and novel supported catalysts for MDA, including but not limited to the variation of the zeolite support material (e.g. ZSM-5, MCM-22, MCM-49, NU-87, TNU-9 etc.), (ii) the structure and nature of the active sites; (iii) thermodynamics of MDA reaction with associated MDA reaction mechanism and performance of various catalysts; and (iv) catalyst deactivation, coke formation and regeneration methods.

Despite extensive characterization studies reported on supported MO_x/ZSM-5 catalysts, many fundamental details such as MO_x anchoring sites, molecular and electronic structures of MO_x and their responses to different reactive environments remain moot. The lack of consensus about the fundamental details of supported MO_x/ZSM-5 catalysts is strongly related to limited *in-situ* studies since most of the characterization measurements were collected under ambient or *ex-situ* conditions where the samples are hydrated and not representative of the catalyst structures present under elevated temperatures and reactant gas(es).

The objective of this review is to critically analyze and summarize recent developments in MDA catalysis with emphasis on fundamental *in-situ* and *operando* spectroscopy studies in the literature on ZSM-5-supported metal oxide MO_x (M=V, Cr, Mo, W, Re and Fe) catalysts. Specifically, this review discusses the anchoring sites of MO_x, molecular and electronic structures of the supported MO_x sites, the nature of the active catalytic site(s) before and during MDA, reaction kinetics, rate-determining steps, and reaction mechanism of MDA.

2. Anchoring sites of surface MO_x species on ZSM-5 support.

A plethora of studies has focused on elucidating the location of the dispersed MO_x sites in the zeolite matrix in ZSM-5-supported catalysts, given the variety of various anchoring sites possible, schematically described in **Figure 2**. Generally, (Al-OH^+-Si) sites with IR band between 3608-3610 cm^{-1} serve as the anchoring sites internally in the 10M pores of ZSM.[42] Outside the pores on the zeolite's surface, the Si-OH (sometimes denoted as Si_{ex}-OH in the literature) indicated by IR band at 3745 cm^{-1}, and Al-OH from extra framework Al (sometimes denoted as Al_{ex} in the literature) or Al_2O_3 nanoparticles with IR bands at 3660, 3783 cm^{-1}, respectively, can also serve as the anchoring sites.[42] It is generally agreed that the metal oxide sites anchor at either the Brønsted acid sites inside the zeolite channels (-Al-OH^+-Si-) and/or at the external (-Si_{ex}-OH), with the

distribution between internal and external anchoring sites dependent on the synthesis method and Si/Al ratio.[9,31,43] In past studies, the anchoring sites of supported MO_x species (such as WO_x, MoO_x and ReO_x) were determined from the titration of residual zeolite protons, where the MO_x species were assumed to have only one type of site.[31,44,45] In contrast, this section on the anchoring sites of supported metal oxides on ZSM-5, emphasized on insights generated via *in-situ* characterization of the catalysts under dehydrated conditions. Studies undertaken in ambient conditions will not be covered since such hydrated catalysts are not relevant to reaction conditions. A detailed discussion of the literature findings is given below, and a summary of anchoring sites for supported MO_x/ZSM-5 catalysts is presented in **Table 1**.

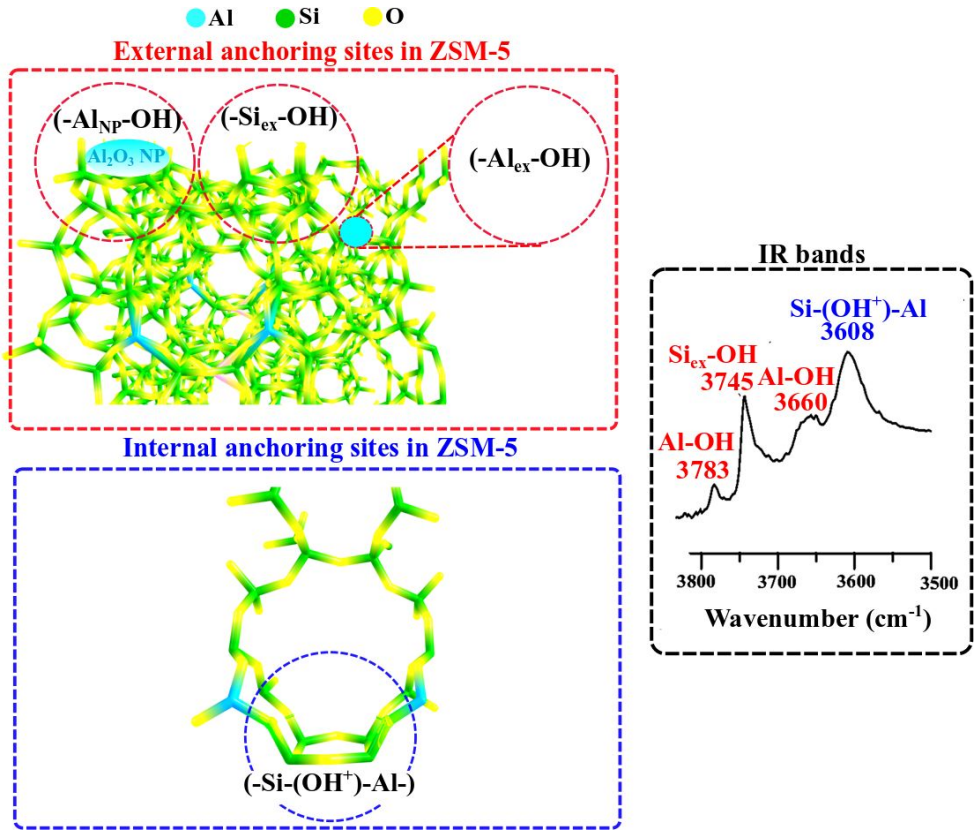

Figure 2. *Types of external and internal anchoring sites and their corresponding IR bands, present in H-ZSM-5 zeolite. Hydrogen atoms are not shown here for clarity.*

Supported VO_x/ZSM-5. The anchoring sites in VO_x/ZSM-5 catalysts are affected by the preparation method, as confirmed via *in-situ* (room temperature measurements after high-temperature treatment, without exposing to air) spectroscopic techniques in various reports.[9,46,47] Using IR spectroscopy (spectra collected at room temperature, under vacuum, after dehydration at 773 K), it was shown that the samples prepared by impregnation mainly led to the consumption of external silanol groups in the zeolite. In contrast, samples prepared via solid-state reaction of VCl_3 and H-ZSM-5 primarily resulted in the consumption of framework Brønsted acid sites. Moreover, a monotonic decrease in the framework Brønsted acid sites was observed, via *in-situ* IR spectroscopy, with an increase in the $V/Al_{framework}$ ratio, along with complete consumption of external silanol groups during solid ion exchange by sublimation of $VOCl_3$ onto ZSM-5.[46] Stoichiometrically, the introduction of each V-atom replaced ~1 proton of the Brønsted acid sites (Al-$(OH)^+$-Si) in the zeolite.

Supported CrO_x/ZSM-5. An *in-situ* diffuse reflectance infra-red Fourier transform spectroscopy (DRIFTS)[48] characterization of supported CrO_x/ZSM-5 (Si/Al=15) catalysts, synthesized by solid-state exchange of various chromium salts (Cr-nitrate, Cr-acetate, Cr-chloride, etc.) and ZSM-5, found that the CrO_x species are mainly present at the Brønsted acid sites within the zeolitic pores, with a small amount of CrO_x species present at the external silanol sites of the ZSM-5 support.[48] In contrast, a recent in-depth study[49] combining computational, *in-situ*, and *operando* spectroscopic characterization (IR, Raman, Ultraviolet-Visible Diffuse Reflectance Spectroscopy (UV-vis DRS)) of supported CrO_x/ZSM-5 catalysts with varying Cr-loading and Si/Al ratios found that CrO_x species preferentially anchors at Si-OH sites on the external surface of the zeolite at higher Cr- weight loading (above 0.5 weight %) and when the Al-framework site concentration in ZSM-5 was low (Si/Al=140).[49]

Supported MoO_x/ZSM-5. It is generally accepted in the literature that both framework Brønsted acid sites (Al-$(OH)^+$-Si) and external silanol (Si-OH) groups serve as the anchoring sites for MoO_x species on ZSM-5.[50,51] However, the migration of the MoO_x between various surface hydroxyl anchoring sites is still unresolved. For example, it was reported from *in-vacuo-in-situ* IR measurements that MoO_x is equally distributed at both framework Brønsted acid sites and silanol hydroxyls for low loading cases (< 3 wt.%) and preferentially anchored at framework Brønsted acid sites for dehydrated catalysts with 6% MoO_x/ZSM-5 (Si/Al=25).[52] In another *in-situ* IR spectroscopy study, on supported 2% MoO_x/ZSM-5 (Si/Al=25) catalysts synthesized by impregnation, it was found that MoO_x migrates from external silanols and extra-framework Al-OH hydroxyls to framework Brønsted acid sites Al-OH^+-Si at elevated calcination temperatures.[53] Preparation from a physical mixture of MoO_3 and ZSM-5, however, indicates the presence of residual framework Brønsted acid sites Al-OH^+-Si even after calcination at elevated temperatures, reflecting a synthesis-dependent anchoring of MoO_x sites.[44,45] It was also assumed that MoO_x anchored as surface Mo_2O_5 dimers at two adjacent framework Brønsted acid sites, but no direct supporting spectroscopic information was provided about the structure of the MoO_x species and the anchoring sites on ZSM-5.[44,45] Moreover, the probability of finding two adjacent Al framework Brønsted acid sites required for anchoring surface dimeric Mo_2O_5 is very low according to Lowenstein's rule.[54] Typically, framework Brønsted acid sites in 10M rings are either isolated or separated by at least two Si atoms as in Al-OH^+-Si-O-Si-OH^+-Al.[55]. Therefore, enough paired Al-OH^+-Si-OH^+-Al sites will not be present for anchoring at high loadings of MoO_x on ZSM-5 making the anchoring of such dimeric sites very unlikely. More recently, systematic computational and experimental studies on supported MoO_x/ZSM-5 catalysts have conclusively elucidated the anchoring sites as a function of Mo loading and zeolite Si/Al ratio with *in-situ* IR.[42,56] The IR

spectra demonstrated that the MoO_x species preferentially anchor at zeolitic Brønsted acid sites for low Mo oxide loading and anchor to external Si-OH sites for higher Mo loadings, indicating external Si-OH sites can also serve as additional anchoring sites. In addition, Mo deposition can also cause some dealumination of the zeolite framework, and a small fraction of MoO_x can also anchor on the extra-framework Al-OH sites. [42,56] These findings were also corroborated by a recent *in-situ* IR spectroscopy study.[57] The MoO_x sites, generated by physical mixing of MoO_3 and H-ZSM-5 followed by calcination, were found to anchor at Brønsted acid sites of the ZSM-5 support.[57] Consequently, the surface MoO_x anchor at multiple surface hydroxyls and not selectively at one kind of surface hydroxyl.

Supported WO_x/ZSM-5. *In-situ* IR study shows that the anchoring sites for WO_x species on ZSM-5 support depends on the preparation method.[9] For WO_x/ZSM-5 catalyst prepared by the solid-state ion exchange method, the Brønsted acid sites Al-OH^+-Si were mainly affected, suggesting anchoring of WO_x species on these sites. The catalysts prepared by the impregnation method, however, were found to be mostly anchored at the external Si-OH surface hydroxyls. In another study[58], where the supported WO_x/ZSM-5 catalyst was prepared by incipient-wetness impregnation of $(NH_4)_2WO_4$ (dried at 393 K for 2 h and calcined at 773 K for 5 h), the effect of WO_x on the Brønsted acidity of ZSM-5 was probed with NH_3-temperature programmed desorption (TPD). Only a small change in the desorption temperature and peak intensity for NH_3 desorption was noticed, suggesting WO_x might be anchored to the Brønsted acid sites of the H-ZSM-5 (Si/Al=38) support. This indirect characterization method, however, was unable to distinguish between Brønsted acidity of the ZSM-5 support and new Brønsted acid sites that might have been created by anchoring of the WO_x species (3 wt.% WO_x, prepared by incipient-wetness impregnation). A different study proposed that the WO_x species requires two framework Brønsted

acid sites on ZSM-5.[31] However, this conclusion was solely based on titration of the residual protons of ZSM-5 support and lacked any direct spectroscopic supporting evidence. In conclusion, identification of anchoring sites in WO_x/ZSM-5 catalysts is, thus, pending modern *in-situ* characterization measurements.

Supported ReO_x/ZSM-5. The anchoring sites of dispersed ReO_x for supported ReO_x/ZSM-5 catalysts have received limited attention. *In-situ* IR studies reported that supported ReO_x species preferably anchor at the zeolitic Brønsted acid sites, with a small amount of ReO_x species also anchoring at the external silanols.[24,59,60] *In-situ* XAS data in the report corroborated the presence of isolated ReO_4 in ReO_x/ZSM-5[24], while no direct evidence regarding the proposed dimeric Re_2O_y species[59] could be found in the literature.. Furthermore, it should be noted that dimeric Re_2O_y species are volatile[61,62] and will not remain on the catalyst surface upon formation, especially at elevated temperatures.[63,64]

Supported FeO_x/ZSM-5. The surface FeO_x species of the supported FeO_x/ZSM-5 catalysts were found to be anchored within the zeolitic pores of ZSM-5 and are dependent on the preparation method. Chemical vapor deposition of $FeCl_3$, followed by washing and calcination, results in dispersed FeO_x/ZSM-5 catalysts at high Fe loading.[65,66] The *in-situ* IR results of these catalysts revealed that the FeO_x species anchored at the framework Brønsted acid sites. Other studies employing solid-state ion exchange and *in-situ* IR revealed the consumption of framework Brønsted acid sites upon anchoring of FeO_x.[9,67] In contrast, *in-situ* IR data of the supported FeO_x/ZSM-5 catalysts, prepared by the impregnation method, evidenced the preferential anchoring of FeO_x species at external Si-OH sites.[9]

Table 1. Reported anchoring sites of surface MO_x species in supported MO_x/ZSM-5 catalysts based on IR spectroscopy.

Catalyst	Synthesis Method	Reported anchoring sites	Ref.
VO_x/ZSM-5	Incipient-wetness impregnation of NH_4VO_3	-Si_{ex}-OH	9
	Solid-state ion exchange	-Al-OH^+-Si-	9
CrO_x/ZSM-5	Incipient-wetness impregnation of CrO_3	-Si_{ex}-OH	9
	Solid-state ion exchange	-Al_{ex}-OH^+-Si-	9
	Solid-state ion exchange	Primary: -Al-OH^+-Si- Secondary: -Si_{ex}-OH	48
	Incipient wetness impregnation of $(Cr(NO_3)_3 \cdot 9H_2O$	-Si_{ex}OH and -Al-OH^+-Si-	49
MoO_x/ZSM-5	Incipient-wetness impregnation of $(NH_4)_6Mo_7O_{24}$	-Si_{ex}-OH	9
	Solid state ion exchange	-Al-OH^+-Si-	9
	Thermal spreading of MoO_3 onto ZSM-5	-Al-OH^+-Si-	57
	Incipient-wetness impregnation of $(NH_4)_6Mo_7O_{24} \cdot 4H_2O$	High loading: -Si_{ex}-OH Low loading: -Al-OH^+-Si-	42
WO_x/ZSM-5	solid-state ion exchange	-Al-OH^+-Si-	9
	Incipient-wetness impregnation of $(NH_4)_{10}H_2(W_2O_7)_6$	-Si_{ex}-OH	9
	Incipient-wetness impregnation of $(NH_4)_2WO_4$	-Al-OH^+-Si-	58
ReO_x/ZSM-5	Vapor-phase exchange of Re_2O_7	-Al-OH^+-Si-	24, 58
	Incipient wetness impregnation of NH_4ReO_4	Primary: -Al-OH^+-Si- Secondary: -Si_{ex}-OH	59
FeO_x/ZSM-5	CVD of $FeCl_3$	-Al-OH^+-Si-	65,66
	Solid state ion exchange	-Al-OH^+-Si-	9,67
	Incipient wetness impregnation $Fe(NO_3)_3.9H_2O$	-Si_{ex}-OH	9

3. Nature of surface MO_x sites in supported MO_x/ZSM-5 catalysts before MDA.

Various literature reports for ZSM-5 supported MO_x catalysts discuss the nature of metal oxide sites within the zeolitic pores. Typically, *in-situ* and *operando* spectroscopic techniques such as Raman, UV-vis DRS, XAS, etc. have been used to directly probe the structure of the dehydrated and oxidized MO_x sites before MDA. Earlier non-spectroscopic characterization studies employing the indirect method of titration of surface hydroxyls, however, have also been applied to propose the structure of the MO_x sites on ZSM-5. A case-by-case discussion of the nature of

surface MO_x sites before MDA in group V-VII metal oxides/ZSM-5 catalysts is given in the following subsections. The reader should keep in mind that the nature of sites in supported heterogenous catalysts has historically remained controversial in the broader catalysis field because of different approaches employed in trying to assign supported MO_x structures. For example, the question of isolated versus dimeric/oligomeric active sites has been heavily debated with regards to CrO_x/SiO_2-type Phillips catalysts. Simple titration study of Si-OH groups by CrO_x suggested the co-existence of both isolated CrO_4 and dimeric Cr_2O_7 species on SiO_2.[68] More recent characterization studies employing direct advanced *in-situ* spectroscopic characterization, however, conclude that only isolated surface CrO_x sites are present on the SiO_2 support.[69,70] Likewise, no consensus exists regarding the nuclearity of active Cu sites in zeolite supported Cu_xO_y catalysts used for selective catalytic reduction of NO_x and methane-to-methanol reactions.[71–73] In this context, we have critically analyzed the state-of-the art literature reports on ZSM-5 supported MDA catalysts and provided our proposals for the structures of the surface MO_x sites on ZSM-5 based on the most advanced supporting data available. We, however, tried to analyze key literature from all sides of the debate to provide the reader with a nuanced understanding of the catalytic active sites in these MDA catalysts. The large variety of anchoring sites on the ZSM-5 support suggests that multiple surface MO_x sites are probably formed for each metal oxide on ZSM-5.

Supported VO_x/ZSM-5. Several molecular structures for dehydrated supported VO_x species on ZSM-5 have been proposed in the literature. Early electron paramagnetic resonance/electron spin resonance (EPR/ESR) measurements evidenced EPR-active V^{4+} oxides present on the zeolite. It was hypothesized that isolated VO^{2+} were present on the cationic sites of zeolites via ESR conducted after various treatments like heat treatment (720 K, 6 h, N_2), adsorption of water, or

adsorption of ammonia.[74,75] A different study[47] proposed the presence of VO^{2+} species on both Brønsted acid sites and external silanols. Note, however, that EPR spectroscopy only detects paramagnetic V^{4+} species that may be present in trace quantities and not V^{5+}/V^{3+} species that are EPR silent. Moreover, interpreting EPR signals in supported catalysts to conclude isolated *vs.* dimeric/oligomeric VO_x sites is challenging, given that even the EPR of V_2O_5 single crystals showed significant deviation from expected EPR patterns and exhibited electron sharing between inequivalent V-V neighbors.[76]

In a relatively-recent *in-situ* characterization study, the presence of isolated dioxo VO_2^+ and dimeric $V_2O_4^{2+}$ species located on cationic sites of zeolites for supported VO_x/ZSM-5 (Si/Al~13.4) were proposed based on *in-situ* FT-IR, *in-situ* Raman and EXAFS.[46] The Raman bands in the 1065-1076 cm^{-1} range were assigned to the terminal V-oxo (V=O) vibration, based on the DFT calculations in the same study. [46] However, experimental Raman of supported VO_x catalysts elsewhere in the literature evidences V=O vibrations at lower wavenumbers.[77] The terminal V=O bond for mono-oxo $O=VO_x$ sites exhibits only a single Raman band in the 1015-1040 cm^{-1} range, which is much lower than 1065-1076 cm^{-1} scale.[78,79] The V=O bonds in dioxo O=V-O-V=O are expected to be longer than the V=O bond in mono-oxo $O=VO_x$ sites and would give rise to V=O vibrations at much lower wavenumbers than 1015-1040 cm^{-1}.[80] Additionally, the dioxo O=V-O-V=O structure would give rise to both v_s and v_{as} V=O (a doublet) as well as V-O-V vibrations, which were not observed. The high wavenumber band at 1065-1076 cm^{-1} reported in reference [46] might either correspond to Si-O-Si vibration or be blue-shifted due to Raman spectrometer not being calibrated. The proposed dimeric surface $V_2O_4^{2+}$ species, if present, cannot be present in significant abundance since the *in-situ* extended X-ray absorption fine structure (EXAFS) spectra[46] does not exhibit a V-V peak in the second coordination sphere (i.e., V-O-V) at ~3 nm.[81] The X-

ray absorption near-edge structure (XANES) part of the spectrum exhibits a clear pre-edge, which is expected for isolated, non-centrosymmetric sites like the mono-oxo $O=VO_3$ sites. As bridged V-O-V bonds form as in dimeric $V_2O_4^{2+}$ sites, the symmetry of the sites should have changed that would lead to a decreased pre-edge intensity.[81] Such a decrease in the pre-edge feature, however, was not observed suggesting that the presence of dimeric surface V_2O_x sites in VO_x/ZSM-5 catalysts is not supported by the XANES spectra.

The *in-situ* UV-vis spectra of dehydrated 3% VO_x/ZSM-5 (Si/Al=15), prepared by incipient-wetness impregnation, exhibited a strong Ligand-to-Metal Charge Transfer (LMCT) band characteristic of V^{5+} species[82] and a high edge energy value (E_g~3.5 eV) in the region of isolated surface $V^{5+}O_x$ sites. Oligomeric $(VO_x)_n$ sites give rise to E_g values of ~2.8-3.2 eV and bulk V_2O_5 exhibits an even lower E_g~2.3 eV.[83,84] The corresponding *in-situ* Raman spectrum exhibits only a single, sharp Raman band at ~1038 cm^{-1} that is characteristic of a mono-oxo V=O stretching vibration,[82] which matches the VO_4 ($O_3V=O$) coordination of dehydrated surface species on other oxide supports.[79,83,85,86]. No supporting evidence was found for isolated, dioxo $OV^{5+}(=O)_2$, which would give rise to two bands (v_s and v_{as}) at lower wavenumber (~1000 cm^{-1}), or dimeric V_2O_x, which would exhibit bridging V-O-V Raman vibrations ~250 cm^{-1} and V-V features in the second coordination of EXAFS, were found. Therefore, it is expected that surface VO_x sites are present within the zeolitic pores of the ZSM-5-supported catalysts as isolated, mono-oxo ($O_3V^{5+}=O$) surface species, as shown in other supported VO_x catalysts. [79,83,85,86] A schematic of the molecular structure of the major dehydrated VO_x site on the ZSM-5 support based on *in-situ* spectroscopic evidence for supported VO_x/ZSM-5 is shown in **Figure 3a**.

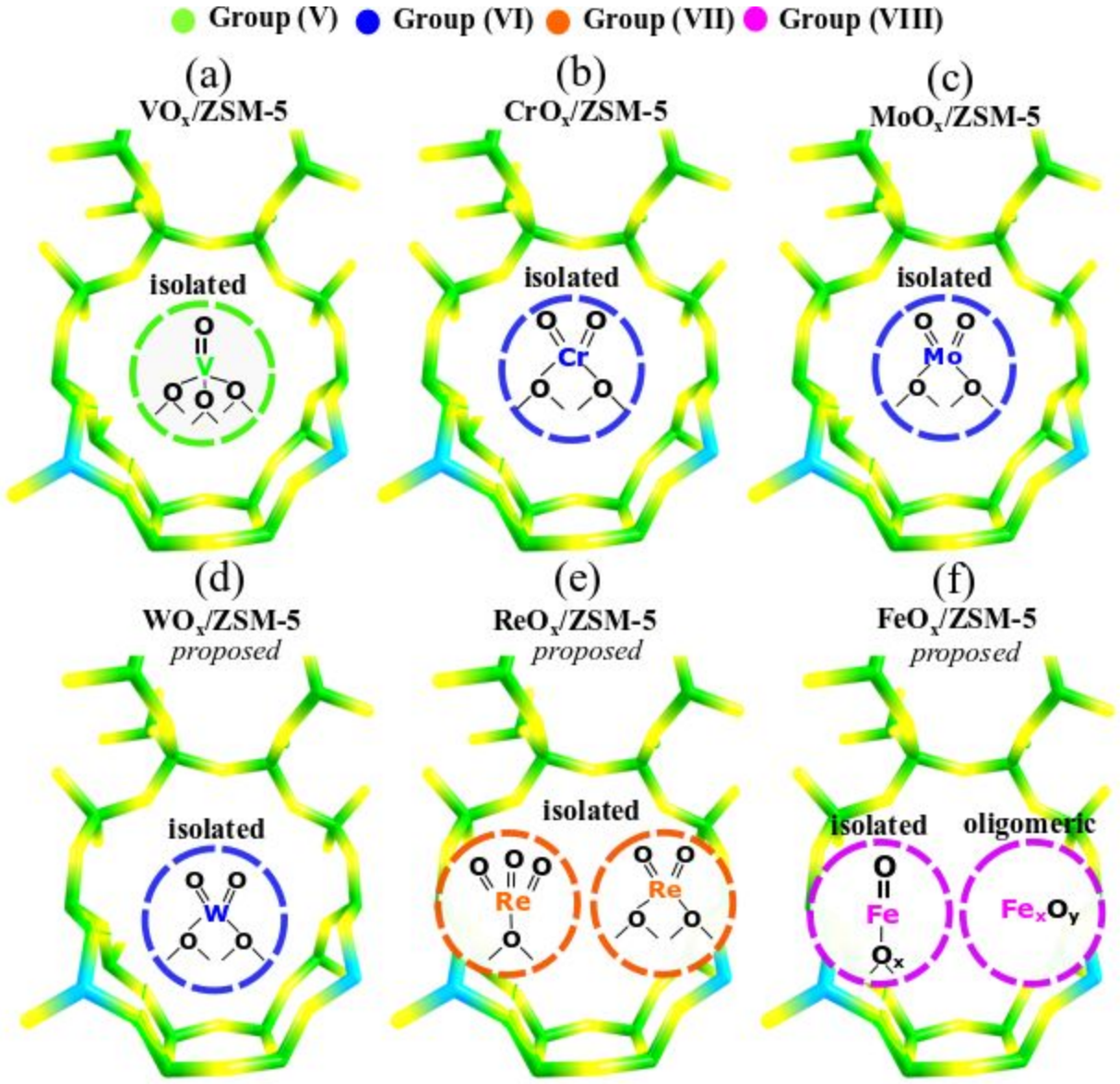

Figure 3. *Schematic summary of molecular structures of the major dehydrated MO_x sites on the ZSM-5 support, based on in-situ spectroscopic (Raman, UV-Vis, x-ray absorption) and DFT. These structures represent surface MO_x anchored within the zeolitic pores of MO_x/ZSM-5 catalysts under dehydrated conditions, before MDA reaction, where MO_x is (a) VO_x, (b) CrO_x, (c) MoO_x, (d) WO_x, (e) ReO_x, and (f) FeO_x. Hydrogen atoms are not shown for clarity. Further details and structures of minor species can be found within respective references of subsections under* ***Section 3****.*

Supported CrO_x/ZSM-5. Early characterization studies employing *in-situ* IR, EPR and Mossbauer spectroscopy under vacuum conditions proposed the presence of both Cr^{+5} and Cr^{+6} cations for the supported CrO_x/ZSM-5 catalysts.[87] It is worth noting, however, that Cr^{+6} can readily

reduce to Cr^{+5} under vacuum and may give rise to Cr^{+5} signals (e.g., EPR) that are artificially induced by the experimental conditions. Employing *in-situ* XAS (sample sealed in polyethene films under inert atmosphere after treatment with air and taken to the beamline, XAS at 295 K),[88] the supported CrO_x/ZSM-5 catalysts prepared via wet-impregnation of Cr-nitrate solution into ZSM-5 were investigated. The presence of Cr-O-Cr coordination indicated the presence of Cr_2O_3 nanoparticles (NPs) for Si/Al ratios of 29-940. In comparison, only isolated surface CrO_x^{6+} sites were evidenced for higher Si/Al ratios (> 940). Based on the intense pre-edge feature in the XANES portion of the XAS spectrum, the possibility of di-grafted, dioxo $O_2Cr(=O)_2$ structures present on the ZSM-5 support was proposed for Si/Al ratios of 29-1900. In the same study, complementary EXAFS of the catalysts with Si/Al ~29-1900 corroborated the presence of significant Cr=O bond character in the first coordination shell, but also evidenced weak Cr-O-Cr coordination as in Cr_2O_3 NPs in the second and third coordination shells.[88] A simplistic schematic, for illustration purpose, of tri-oxo CrO_x structure has also been proposed in the literature, where the bridging Cr-O-support bond shares an electron with one of the three terminal Cr=O bonds.[89] This report warrants some additional discussion since an isolated trioxo $Cr(=O)_3$ structure would be expected to give rise to four Raman vibrations located at ~908 (ν_s), 933 (ν_{as}), 947 (ν_{as}), and 955 (ν_{as}) cm^{-1} that have been reported for the gas phase tri-oxo $CsBrCr(=O)_3$ reference compound.[90] Without confirmation from *in-situ* Raman spectroscopy, the surface tri-oxo $(O=)_3CrO$ structure cannot be validated and seems highly improbable. The number of Cr=O oxo bonds, however, can be confirmed with Raman spectroscopy during isotopic $^{18}O_2$-$^{16}O_2$ exchange since a trioxo $(Cr=O)_3$ functionality will give rise to band splitting to 4 bands from the isotopic permutations($(=^{16}O)_3$, $(=^{16}O)_2(=^{18}O)$, $(=^{16}O)(=^{18}O)_2$ and $(=^{18}O)_3$).[91] Recently, dehydrated supported CrO_x/ZSM-5 catalysts prepared by solid-state reaction (Si/Al=15, Cr/Al=0.5, 1 and 1.5) and were characterized

with Raman and UV-Vis DR spectroscopy.[48] The Raman band at ~375 cm^{-1} was assigned to oligomeric CrO_x. However, elsewhere in the literature, a similar band is actually assigned to the ZSM-5 support.[92,93]

In a more recent in-depth study, the dehydrated supported CrO_x/ZSM-5 catalysts were thoroughly characterized via *in-situ* UV-Vis DR, IR and Raman spectroscopy.[49] For 1 wt % CrO_x/ZSM-5 (Si/Al = 15, 25 and 40) catalyst samples, under O_2 flow at 383 K, Raman bands at 964 and 1033 cm^{-1} were observed, which were assigned to the di-oxo $O_2Cr(=O)_2$ and mono-oxo $O_4Cr(=O)$ structures within the zeolitic pores, anchored on to Brønsted acid sites. For lower concentration of Al (Si/Al = 140), new bands at 984 and 1017 cm^{-1} were present, which correspond to dioxo $O_2Cr(=O)_2$ and mono-oxo $O_4Cr(=O)$ structures on Si-sites, respectively, on the external surface of ZSM-5. This observation suggests that lower Al concentration force CrO_x to become anchored on the Si sites of the external surface. Further, it should be noted that these spectra were different from the spectra obtained under the same O_2 flow but at a higher temperature of 773 K. At 773 K, for all Si/Al ratios (25, 40 and 140), the catalysts exhibit Raman vibrations at 984 and 1017 cm^{-1}, indicating that exposure to gas-phase O_2 at elevated temperatures forces the Cr oxide species within the zeolite pores to migrate to the external surface of the zeolite.[49] Migration was only observed when Cr loading was higher than 0.5 wt% since no shift in Raman bands was noticed at lower Cr loading.[49] A schematic of the molecular structure of the major dehydrated CrO_x sites based on *in-situ* spectroscopic (Raman, UV-Vis, x-ray absorption) and DFT for supported CrO_x/ZSM-5 is shown in **Figure 3b**.

Supported MoO_x/ZSM-5 Multiple MoO_x structures have been proposed for the supported MoO_x/ZSM-5 catalysts. From *in-situ* XAS characterization,[45] catalysts prepared by thermal spreading of MoO_3 onto a ZSM-5 (Si/Al=19) support, bridging Mo-O-Mo bonds in the second

coordination shell (Mo-O-Mo) were not observed. It can be argued that dimeric $(Mo_2O_5)^{2+}$ sites were present, and that the absence of a detectable Mo-O-Mo feature was related to destructive interference of the EXAFS signals from Mo and Al neighbors. However, Al is a much lighter element than Mo and, thus, the weaker EXAFS scattering from the Al sites cannot destructively interfere with the much stronger EXAFS scattering from the Mo sites. In the same study, the *in-situ* visible Raman spectra exhibited bands at 970 and 1045 cm^{-1}, which were tentatively assigned to dimeric and isolated MoO_x sites, respectively. Dimeric Mo_2O_5 sites were proposed in another study, where *in-situ* Raman bands at 868 and 962 cm^{-1} were assigned to the Mo-O-Mo stretching mode of dimers and the terminal M=O stretch in isolated mono-oxo $O_4Mo{=}O$ sites, respectively.[94] In contrast, however, the vibration at 868 cm^{-1} is characteristic of bridging Mo-O-Al/Si vibrations and the vibration at 962 cm^{-1} is related to terminal Mo=O bonds (most likely dioxo MoO_4 sites).[95–97] The oxidation state of the surface MoO_x sites, which some authors tried to characterize with EPR, was not resolved because concrete evidence for the proposed oxidation states could not be obtained.[50] A more recent *in-situ*/*operando* XAS spectroscopic study found that the dehydrated MoO_x/ZSM-5 catalyst exhibits a strong pre-edge feature with a featureless post-edge regime, which is similar to the Na_2MoO_4 reference compound consisting of isolated MoO_4 sites.[98] Consequently, it was proposed that the dehydrated MoO_x/ZSM-5 catalyst predominantly contains monomeric $[MoO_4]^{2-}$ species and that a minor amount of dimeric Mo-oxo species may also be present without any supporting evidence. In another *in-situ*/*operando* XAS study of MoO_x/ZSM-5 catalysts, it was reported that at low Mo loading (< 2 wt. % Mo), only the dispersed Mo-complexes are present within the zeolitic pores, whereas at high Mo loading (5 wt. % Mo) large Mo clusters are also present on the external surface of the zeolite support.[99]

Rigorous characterization studies integrating *in-situ* Raman, UV-vis and DFT calculations have provided a more firm picture of the nature of the dehydrated surface MoO_x sites on ZSM-5.[42,56] The isolated nature of the dehydrated surface MoO_x sites on ZSM-5 was demonstrated with *in-situ* UV-vis studies that exhibit a high E_g value of ~4.9 eV, which is significantly higher than the E_g value expected for dimeric Mo_2O_x (~4.0-4.2 eV) and oligomeric MoO_x (~3.5 eV) clusters, and reflects the exclusive presence of isolated surface MoO_x sites.[42,56] The corresponding *in-situ* Raman spectra of the dehydrated supported MoO_x/ZSM-5 catalysts revealed that five distinct surface MoO_x species were present on the ZSM-5 support with the relative population of each surface MoO_x structure dependent on both the MoO_x loading and the Si/Al ratio: (i) isolated, di-oxo $(OH)O_2Mo(O=)_2$ on single Al site inside the 10M ring, (ii) isolated di-oxo $O_2Mo(O=)_2$ on two Al sites within the 10M ring (iii) isolated di-oxo $O_2Mo(O=)_2$ on external silanols, (iv) isolated, mono-oxo MoO_5 species on Al_2O_3 nanoparticles/clusters on the external surface, (v) isolated, mono-oxo MoO_5 at external defect sites (Si_{ex} and Al_{ex}). The resulting molecular structures are summarized in **Figure 4**. The molecular structural assignments were assisted by detailed DFT calculations (see references [42,56] for the details). Additionally, crystalline MoO_3 NPs can form at high Mo loadings when all the anchoring sites on ZSM-5 are completely titrated. These *in-situ* spectroscopic findings clearly demonstrate the co-existence of multiple types of "isolated" surface MoO_x sites on the ZSM-5 support and rule out possibility of dimeric Mo_2O_x species . A schematic of the molecular structure of the major dehydrated VO_x site on the ZSM-5 support based on *in-situ* spectroscopic (Raman, UV-Vis, x-ray absorption) and computational insights for supported MoO_x/ZSM-5 is shown in **Figure 3c.**

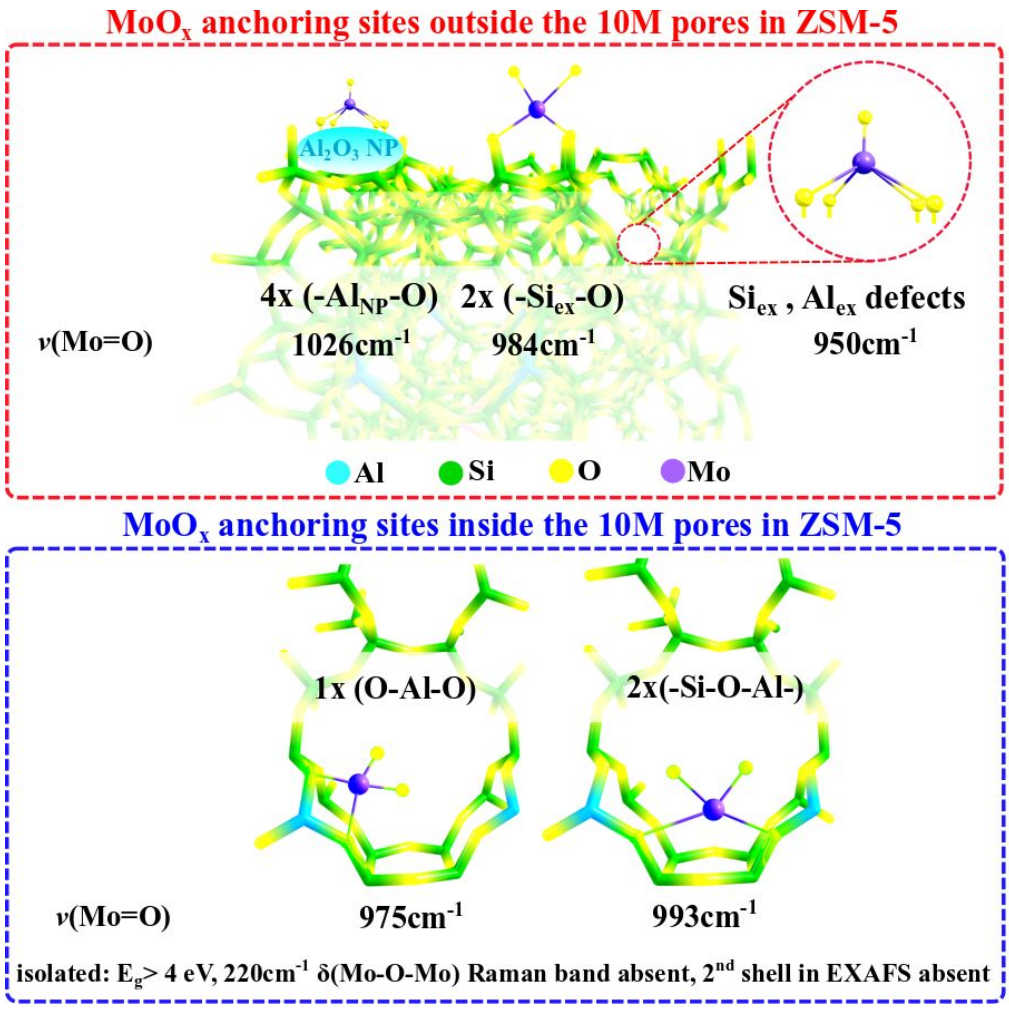

Figure 4. *Unique isolated surface MoO_x sites present in MoO_x/ZSM-5 catalysts. The motivation for the schematic has been drawn from the in-situ spectroscopic and DFT studies reported in references* [42,56].

Supported WO_x/ZSM-5. There is a general agreement in the literature regarding the nature of the dispersed WO_x sites present in dehydrated supported WO_x/ZSM-5 catalysts.[30,31] UV-vis DRS analysis has shown that the surface WO_x sites are isolated owing to the very high E_g value ~5.8 eV (LMCT ~210 nm).[30,31] Tungsten oxide UV-Vis E_g values > 5.0 eV correspond to isolated WO_x sites since the E_g value for dimeric W_2O_x (~4.0 eV) and oligomeric WO_x (~3.5 eV) are significantly lower. This conclusion is further supported by *in-situ* EXAFS measurements that did not exhibit a second coordination shell comprising W-O-W linkages.[82,100] The *in-situ* Raman spectrum of the

dehydrated supported WO_x/ZSM-5 catalyst exhibited two Raman bands at ~990 and 1020 cm^{-1} that have been assigned to isolated dioxo $O_2W(O=)_2$ and mono-oxo $O_4W=O$ species on ZSM-5,[82] respectively, that match WO_4 and WO_5 vibrations of isolated WO_x species on other oxide supports.[101–104] A schematic of the molecular structure of the most likely dehydrated WO_x site on the ZSM-5 support based on *in-situ* spectroscopic (Raman, UV-Vis, x-ray absorption) for supported WO_x/ZSM-5 is shown in **Figure 3d**.

Supported ReO_x/ZSM-5. Based on *in-situ* Raman and XAS measurements, it was proposed that supported ReO_x species on ZSM-5 were present as isolated trioxo $ORe(=O)_3$ species anchored to one site associated with framework alumina (e.g., Si-O*-Al-O*-Si).[24,59] The absence of bridging Re-O-Re vibrations for dimeric Re_2O_x, which are expected at ~456 (v_s) and ~185 (δ) cm^{-1} in the Raman spectra, and the absence of Re-O-Re in the second coordination sphere in the EXAFS spectra demonstrate that the surface ReO_x sites are indeed isolated on the ZSM-5 support.

More recent *in-situ* UV-Vis and Raman characterization studies have provided additional insights about the dehydrated surface ReO_x sites present in the supported 3% ReO_x/ZSM-5 (Si/Al-15) catalyst.[82] The *in-situ* UV-vis spectrum exhibit an E_g value of ~5.0 eV that is significantly higher than the E_g value of oligomeric $(ReO_x)_n$ structures at 2.8-3.0 eV and confirms the isolated nature of the surface ReO_x sites on ZSM-5.[84] The corresponding *in-situ* Raman spectra of the dehydrated ReO_x/ZSM-5 catalyst possessed two vibrations at 975 and 1010 cm^{-1} that were assigned to v_{as}(Re=O) and v_s(Re=O) vibrations, respectively, of a structure containing multiple Re=O oxo bonds. Additional studies involving isotopic ^{18}O-^{16}O exchange and DFT calculations are needed to determine the number of Re=O oxo bonds for the supported ReO_x/ZSM-5 catalysts.[63,6478] A schematic of the molecular structure of the most *likely* dehydrated ReO_x sites on the ZSM-5

support based on *in-situ* spectroscopic (Raman, UV-Vis, x-ray absorption) for supported ReO_x/ZSM-5 are depicted in **Figure 3e**.

Supported FeO_x/ZSM-5. Preliminary studies on catalysts prepared via CVD or solid-state ion exchange, to achieve a high Fe/Al exchange ratio, evidenced various FeO_x sites (isolated (O-Fe-$(OH)_2$), isolated (O-Fe=O) in distorted tetrahedral coordination, oxygen-bridged dimeric $Fe_2O_3(OH)_2$, oligomeric FeO_x clusters, and small Fe_2O_3 nanoparticles).[65,105] A recent *in-situ* XAS study, where the absorption data were fitted to crystalline reference compounds, that the FeO_x sites prior to any treatment were present as a mixture of crystalline hematite (Fe^{3+}, α-Fe_2O_3) and magnetite (Fe^{2+}, Fe^{3+}), Fe_3O_4) phases.[106] Upon heating in a He environment to high temperature, the iron oxide structure was reduced to wüstite (Fe^{2+}, FeO).[106] This study, however, could not ascertain if dispersed phases of surface FeO_x sites or clusters were also present in the catalyst since XAS is a bulk characterization technique that averages the signal over all types of FeO_x in the catalyst. Further structural insights are needed with application of molecular spectroscopy that can distinguish between the different types of FeO_x that may be present in the ZSM-5 support (e.g., Raman spectroscopy). A schematic of the molecular structures of the most *likely* dehydrated FeO_x sites on the ZSM-5 support based on *in-situ* spectroscopic (x-ray absorption) for supported FeO_x/ZSM-5 are shown in **Figure 3f**.

4. Nature of surface MO_x sites in supported MO_x/ZSM-5 catalysts <u>during</u> MDA:

Only a few *in-situ*/*operando* spectroscopic characterization studies have been reported on the state of the surface MO_x sites in supported MO_x/ZSM-5 catalysts during MDA. This is a consequence of the few characterization techniques that can operate under the extreme MDA reaction conditions of 973-1073 K. At such high temperatures, only XAS, XRD and Raman spectroscopy can provide

detailed structural information. Other characterization techniques, however, can be applied at much lower temperatures either before or after reaction.

Supported VO_x/ZSM-5. Only a limited number of studies have reported on the nature of the VO_x site in supported VO_x/ZSM-5 catalysts during MDA. *In-situ* X-ray photoelectron spectroscopy (XPS) surface analysis[7] of supported VO_x/ZSM-5, under vacuum conditions before and after reaction with methane at 1023 K for 3-4 hours (without exposing the samples to air after treatment), found the presence of reduced V^{3+} cations on the spent supported VO_x/ZSM-5 catalysts. The local geometry and coordination number of these cations, however, cannot be provided by XPS electron spectroscopy.

Supported CrO_x/ZSM-5. Little has been reported on the structure of the activated CrO_x/ZSM-5 catalysts during MDA. An *in-situ* XPS study (samples were treated under the reaction environment, followed by XPS measurements under ultra-high vacuum, without exposing to atmosphere) with a supported 2% CrO_x/ZSM-5 (Si/Al = 25) catalyst showed that the initial Cr^{6+} oxide sites became partially reduced under reaction with methane and converted to Cr^{3+} oxide sites that remain catalytically active during methane dehydroaromatization at 1023 K.[7] A recent *operando* Raman spectroscopy study during MDA along with computational insights,[49] found that the Raman band at 1033 cm^{-1} from Cr^{+6} mono-oxo species (O_xCr^{6+}=O) anchored at framework [AlO_4] sites disappeared, suggesting reduction, with appearance of a new Raman band at 1062 cm^{-1} from organic deposits. The exact nature of the surface Cr sites on ZSM-5 under reaction conditions (CrC_x vs $CrOC_x$) has still not been elucidated, but the initial Cr^{+6} sites reduce to Cr^{+3}.

Supported MoO_x/ZSM-5. Multiple *in-situ* and *operando* [42,56] spectroscopic studies have focused on determining the nature of the active surface Mo sites during the MDA reaction.[57,98] It is worth noting that since most of the *operando* spectroscopy studies used XAS to characterize the catalyst,

the presence of crystalline MoO_3 NPs cannot be ruled out which complicates the XAS analysis. Additionally, MoO_3 NPs are too large to fit into the pores of ZSM-5 and can easily be converted to large MoC NPs, blocking the pores.[56] Unless Raman spectroscopy was employed to characterize the initial state of the MoO_x in ZSM-5, the presence of crystalline MoO_3 NPs in the starting material would not be known. *Operando* XAS studies revealed that during the MDA reaction, the surface MoO_x sites on the ZSM-5 support: (1) partially carburized to intermediate MoO_xC_y oxycarbide clusters, (2) subsequently carburized to MoC_x clusters at longer reaction times, and (3) finally detached from the zeolitic pore to aggregate into $Mo_{1.6}C_3$ clusters, which was coincident with the maximum benzene production.[107] The $Mo_{1.6}C_3$ clusters, predominantly on the outer zeolite surface, were then observed to grow further, which appears to be the primary cause of catalyst deactivation. Note that catalyst deactivation from hydrocarbon deposition was recently shown to be reaction parameter-dependent, with higher methane pressures stabilizing the supported Mo/ZSM-5 catalyst.[107] Moreover, MoC_x agglomeration was shown to be reversible via *operando* Raman spectroscopy, with the initially isolated surface MoO_x sites essentially completely restored by treatment with gas-phase oxygen post MDA reaction that fully restored the catalytic performance of the supported Mo/ZSM-5 catalysts.[42,56] Both experimental findings and computational calculations confirm the presence of reduced Mo species such as MoO_xC_y and MoC_x, which serve as the active sites during the MDA reaction.[108–112] A recent detailed study employing ^{13}C-NMR with isotopically-labelled $^{13}CH_4$ showed that after activation of 2% MoO_x/ZSM-5 and subsequent switching to $^{12}CH_4$ (with an Ar purge in between) produced a significant amount of ^{13}C containing benzene molecules. More than 70% of the benzene molecules formed after the first $^{12}CH_4$ pulse contained at least one ^{13}C atom, indicating the dynamic and active roles of MoO_xC_y, Mo_xC_y and confined carbonaceous species during MDA.[110]

Supported WO_x/ZSM-5. *In-situ* XAS[31] and *ex-situ* high resolution transmission electron microscopy (HR-TEM)[113] studies found poorly-ordered WC_y (~0.6-1 nm) present inside the zeolitic pores for WO_x/ZSM-5 catalysts during MDA. An *in-situ* XPS study examined the oxidation state of WO_x species on the ZSM-5 support after exposing the catalyst to MDA reaction environment for different amounts of time.[7] After 2 h of reaction, slight decreases in the binding energy of W $4f_{7/2}$ and W $4f_{5/2}$ were observed that are consistent with the formation of W^{+5} oxides. Further exposure to MDA reaction environment (~13 h) showed an additional shoulder ~33.5 eV, corresponding to W^{+4} site. Interestingly, this study did not evidence the formation of WC_x via *in-situ* XPS investigation. Further information on the nature of active surface WO_x sites during MDA is not available, and additional *in-situ* characterization studies using IR, Raman, XAS, and UV-vis DRS are needed as a function of the synthesis method to bridge this information gap.

Supported ReO_x/ZSM-5. The active component of supported ReO_x/ZSM-5 for MDA has attracted little attention in the literature. An *in-situ* XAS study[24] observed that surface ReO_x species converted to metallic Re clusters ~8.2 Å in size, at the initial stage of benzene formation. Given that ~8.2 Å is comparable to the pore size of the ZSM-5 support, it is not clear from this study if the reported Re^0 clusters were observed outside or inside the pores. The facile reduction of $Re^{+7}O_x$ to Re^0 in reducing environments is well known.[62]

Supported FeO_x/ZSM-5. FeO_x/ZSM-5 catalysts were also studied via *operando* XAS.[106] It was found that benzene only formed after a particular XANES feature was observed.[106] Although the XANES spectrum was similar to that of the reduced form of iron, some unique features, however, did not match any of the measured reference compounds (Fe_3C, Fe_2C_5, or Fe foil).[106] Therefore, the unique XANES feature was tentatively assigned to a reduced/metallic iron phase that can include variable amounts of oxycarbidic carbon (e.g., FeO_xC_y) that was also corroborated with the

resemblance of the FT-EXAFS spectrum taken at the end of the MDA reaction with the spectrum of Fe_5C_2 and Fe_3C standards (similar position of the Fe–C and Fe–Fe scattering paths).[106] Facile reduction of iron oxide to metallic Fe^0 in reducing environments is well established.[114–116] In contrast, only a slightly reduced form of iron oxide (Fe_3O_4) was reported from *in-situ* XPS and EPR studies (catalyst conditioned under MDA reaction at 973 K, spectra collected at room temperature) and formation of carbidic/oxy-carbidic Fe-clusters were not detected.[7,117] In the above studies, the presence of Fe_3O_4 phase in the MDA reaction mixture treated catalyst was confirmed by matching the XPS and EPR spectra of the treated catalysts with the signals of Fe_3O_4 bulk phase in the literature.

5. Activity and structure-function relationships of MO_x/ZSM-5 catalysts towards MDA:

Comparison of MDA performance of MO_x/ZSM-5 catalysts. For a detailed comparison of steady-state catalytic MDA performance of various transition metal-oxide-based ZSM-5-supported catalysts, the readers are directed to an existing review paper in the MDA literature.[41] Although, in the mentioned article, the catalysts' performance have been compared under different reaction environment, one can clearly see that the MDA activity of MoO_x/ZSM-5 catalyst towards benzene production is much higher relative to most other MO_x/ZSM-5 catalysts. In the current review, we have tried to critically analyze MDA catalysis literature to generate insights based on reports employing similar reaction conditions or reports where all pertinent experimental information is explicitly reported for us to normalize their data. We compared the benzene production rate per metal atom (turnover frequency (TOF), s^{-1}) for the supported group V-VIII oxide/ZSM-5 catalysts in **Figure 5 (left-a)** and benzene selectivity in **Figure 5 (left-b)**. For the TOF calculation, the reported weight loading of the respective metal atoms was utilized from the original reports.[9,24]. Although it is theoretically possible to back-calculate the TOF from literature

reports if reaction conditions, kinetic parameters and metal oxide loadings are known, we caution the reader against it. TOF should only be calculated when only a single type of site is present, corroborated by molecular spectroscopy (Raman). For example, in a catalyst with a known Mo-loading, if a mixture of crystalline and dispersed phase Mo-sites are present, the CH_4 conversion or C_6H_6 production per Mo atom cannot be calculated accurately. Since Mo in crystalline MoO_3 is not active for MDA but ZSM-5 confined Mo sites are, using theoretical Mo-loading will yield erroneous TOF values. Please see **Table 2** and relevant discussion in the following sub-section.

Figure 5 (left-a) suggests that the supported ReO_x/ZSM-5 and MoO_x/ZSM-5 catalysts exhibit the highest benzene production TOF values amongst group V-VIII catalysts, with the supported ReO_x/ZSM-5 catalyst just barely more active than MoO_x/ZSM-5. Although the specific activity of the supported ReO_x/ZSM-5 catalyst can be slightly higher than that of the supported MoO_x/ZSM-5 catalyst for the MDA reaction, the potential volatilization of ReO_x species during calcination, MDA reaction and catalyst regeneration compromises the practical use of supported ReO_x-based catalysts. MDA activity, which is indicated by the trend in TOF for benzene production over supported MO_x/ZSM-5 catalysts can be summarized as follows: ReO_x/ZSM-5 ~ MoO_x/ZSM-5 > WO_x/ZSM-5 ~ FeO_x/ZSM-5 > VO_x/ZSM-5 > CrO_x/ZSM-5. Next, the selectivity to benzene is compared in **Figure 5 (left-b)** and shows that CrO_x/ZSM-5, MoO_x/ZSM-5 and FeO_x/ZSM-5 exhibit similar selectivity values of ~70-75%, WO_x/ZSM-5 and ReO_x/ZSM-5 ~ 50-55%, and VO_x/ZSM-5 ~ 30%. Note that the reported selectivity in the case of ReO_x/ZSM-5 is for C_6-C_{11}, and not solely for C_6H_6.

Structure-function (or nature-performance) relationships can be envisioned for the three most active catalysts (ReO_x/ZSM-5 ~ MoO_x/ZSM-5 > WO_x/ZSM-5) by correlating the *operando* Raman spectroscopy data available in the literature,[84] with the trend in TOF values reported in **Figure 5**

(**left-a)**. For each catalyst, the initial molecular structure of the metal oxide site present within the 10M ZSM ring is shown in **Figure 5(center)**. The *operando* Raman spectra **Figure 5(right)** were used to track the diminishing M=O bands as the metal oxide sites carburized with increasing MDA reaction time. T_{red} corresponds to the temperature that M=O Raman bands completely vanished, while T_{C6H6} corresponds to the temperature that benzene was first detected in the MS. *Operando* Raman data suggests that the tri-oxo ReO_4/ZSM-5 sites (1013 cm^{-1}) reduced at 500 °C, followed by reduction of di-oxo MoO_4/ZSM-5 (993 cm^{-1}) at ~680-690 °C, and di-oxo WO_4/ZSM-5 (1024 cm^{-1}) at above 700 °C. Severe fluorescence was observed for the WO_x/ZSM-5 above 700 °C, making it hard to ascertain the exact T_{red}. Likewise, T_{C6H6} was 664, 781, and 814 °C for ReO_x/ZSM-5, MoO_x/ZSM-5, and WO_x/ZSM-5 catalysts, respectively. The trends in reducibility of the initial dispersed phase, isolated metal oxide sites confined within the ZSM-5 pores, and the benzene production temperatures correlate strongly. In fact, for the Mo/ZSM-5 catalyst with well-defined MoO_x sites, experimental and computational study evidenced that differences in geometries and electronic properties of Mo carbide structures formed from distinct MoO_x anchored on Al and Si sites yielded differences in their catalytic properties.[42] Specifically, the CH_4 activation energy over the Mo carbide anchored on the double Al-atom site was calculated to be 112 kJ mol^{-1}, while it was ~140 kJ mol^{-1} for the Mo carbide anchored on Si sites.[42] Therefore, special attention should be paid to synthesis and in-depth characterization of initial oxide forms of the ZSM-5 supported catalysts.

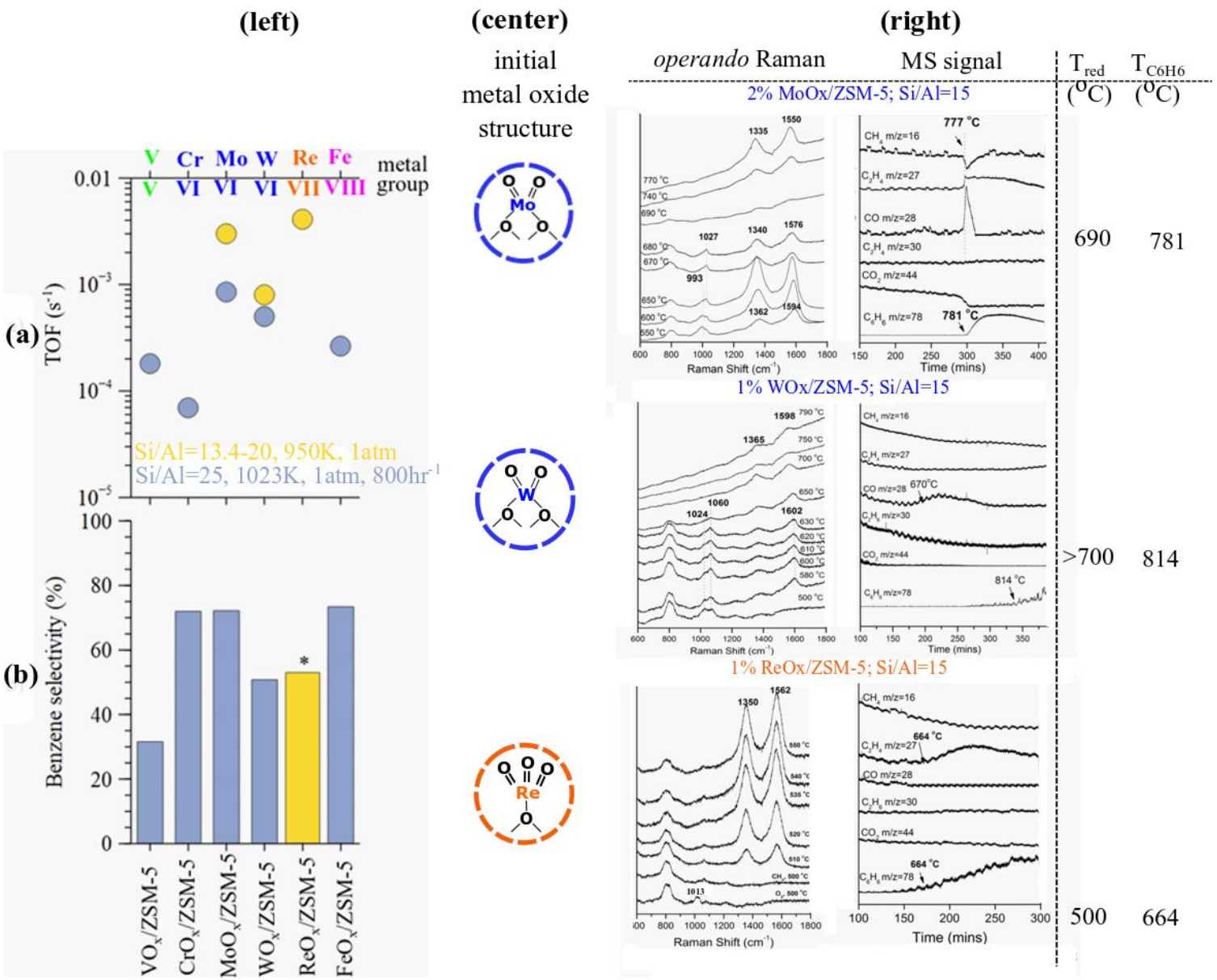

Figure 5. (Left-a) shows benzene production TOF values for group V-VIII supported MO_x/ZSM-5 catalysts. Experimental details for Si/Al =25 can be found in reference [9] and Si/Al = 13.4-20 in reference[24]. For Si/Al=25, the highest reported CH_4 consumption TOF was divided by the stoichiometric factor of six to approximate the benzene production TOF. Lastly, for Si/Al=13.4, the CH_4 GHSV is not reported, and relevant experimental details are not available to approximate the value. (Left-b) indicates the selectivity towards benzene production, taken from references indicated in Figure 5(Left-a). * indicates that the reported selectivity is for C_6-C_{11}, and not solely C_6H_6 as for the other catalysts.(Center) shows the molecular structures of isolated MO_x within the 10M rings of ZSM-5 support prior to MDA reaction. (Right) shows operando Raman spectroscopy, adapted from reference [84] of the three best MDA catalysts Re~Mo>W, correlating the reducibility of the initial isolated metal oxide site with benzene light-off temperature. The T_{red} values pertain

to the temperature where M=O bond completely disappears and T_{C6H6} values refer to temperature that benzene production is first observed

Factors affecting MDA performance of MoO_x/ZSM-5 catalysts. The relative performance comparison of various group V-VIII transition metal catalysts in the previous section shows that Mo-based catalysts exhibit high activity and stability. Hence, we further analyze various factors (material and process) that can affect the MDA performance of MoO_x/ZSM-5 catalysts. The literature reports that included pertinent experimental details are summarized in **Table 2** along with key parameters. **Table 2** highlights significant variability in MDA activity and selectivity of MoO_x/ZSM-5 catalysts across the literature. Nevertheless, the following general conclusions can be drawn from the comparison of data (CH_4 conversion and C_6H_6 selectivity) summarized in **Table 2**.

a) *Effect of Mo loading:* The loading of Mo in supported MoO_x/ZSM-5 catalysts plays a crucial role in determining the catalyst's performance towards MDA reaction. The CH_4 conversion goes through a maximum with increasing Mo weight loading, reaches the maximum conversion at ~3-4 wt.% loading, beyond which conversion drops. [118, 119] This trend in CH_4 conversion can be related to the nature of the MoO_x sites in the catalyst. At low loading (From 0 to ~3-4 wt.%), Mo-oxide is largely present as dispersed, isolated MoO_x sites confined within the zeolitic pores, which are known to be selective active sites for C-H activation. After 3-4% weight loading, further increase in the Mo content results in the formation of crystalline MoO_3 particles (nano- and micro scale) mostly on the external surface of the zeolite, which corresponds to the decreased CH_4 activity. The maximum Mo loading beyond which MoO_3 NPs are formed, however, can be above 3-4 wt.% in certain cases depending on the Al sites, which in turn depend on the Si/Al ratio of

the ZSM-5 support These crystalline MoO_3 are known to form coke on the external surface, which blocks the selective active sites within the zeolitic pores. Although carbided Mo sites are present during MDA reaction, the initial dispersion and structure of MoO_x sites are crucial in determining the observed catalytic performance. On the other hand, the C_6H_6 selectivity exhibits a very low dependency on Mo loading. The selectivity value increases only slightly with Mo loading (up to 3-4 wt.% loading) and remains approximately constant thereafter.

b) *Effect of Synthesis technique:* Incipient wetness impregnation (IWI) of an aqueous solution of $(NH_4)_6Mo_7O_{24}$ into ZSM-5 support, followed by oxidative calcination is the most used synthesis technique for MoO_x/ZSM catalyst preparation. When done carefully, the IWI method can result in uniform dispersion of the MoO_x phase into the ZSM-5 support. The higher dispersion of MoO_x species from IWI synthesis most likely responsible for the higher MDA activity of those catalysts compared to the ones synthesized via solid-state ion exchange of $MoCl_3$ or a mechanical mixing of MoO_3 with ZSM-5 support.[9] In the latter synthesis method, residual crystalline MoO_3 nanoparticles are always present and adversely affect the MDA performance. Recently, novel synthesis approach of wetness impregnation assisted with additional treatment in rotavapor, microwave and ultrasound resulted in catalysts with appreciably higher MDA activity, tested up to 4 hours of time-on-stream (TOS). Moreover, solvothermal synthesis utilizing 10 v% ethanol/water as solvent has also been reported to yield catalysts that were more active towards MDA compared to the IWI catalyst, tested up to 15 hours of TOS.[120] Catalysts synthesized using solvothermal approach were claimed to have a higher dispersion of the MoO_x sites on ZSM-5 in the freshly prepared catalysts. Having said that, additional catalyst

characterization studies are required under *in-situ* and *operando* conditions to corroborate the exact reason behind superior performance of catalysts prepared via advanced synthesis techniques instead of the traditional IWI. Additionally, one more investigation compared the effect of utilizing hexamolybdate $[(C_4H_9)_4N]_2Mo_6O_{19}$ *vs.* heptamolybdate $(NH_4)_6Mo_7O_{24}\cdot 4H_2O$ as the Mo-oxide precursor and found that when hexamolybdate is used as precursor, the C_6H_6 selectivity is much improved. [43]

c) *Effect of Si/Al ratio:* The Si/Al ratio, which controls the acidity of the zeolite support and the dispersion of the supported metal oxide phase is a crucial parameter in MDA performance of MoO_x/ZSM-5 catalysts: higher acidity ZSM-5 support with low Si/Al ratio generally leads to a greater number of surface MoOx sites and higher MDA activity. The literature converges on the understanding that higher the amount of Brønsted acid sites (i.e low Si/Al ratio), higher the dispersion of isolated MoO_x sites within the zeolitic pores will be, which leads to superior MDA activity from the dispersed Mo sites confined within the ZSM-5 pores.[8,121] This trend further highlights the relevance of characterizing and understanding the nature of dispersed phase sites in MDA catalysts.

d) *Effect of reaction pressure:* Only a limited number of studies have undertaken examining the effect of reaction pressure on the MDA performance of MoO_x/ZSM-5 catalyst. Recently, it was reported that with increasing reaction pressure, both CH_4 conversion and C_6H_6 selectivity values increase. [107] The positive effect of higher reaction pressure towards MDA performance was attributed to the decrease in coke formation/catalyst deactivation rate. Higher pressure aiding MDA kinetics was surprising, as higher pressures are expected to shift the reaction towards the reactant's side, given the stoichiometry of 6 moles of CH_4 reactant forming 10 moles of product (1 benzene, 9 hydrogen).

Table 2. MDA reaction performance of Mo/ZSM-5 catalysts reported in the literature. Parameters summarized in the table include Mo loading, catalyst synthesis techniques, Si/Al ratio, and total reaction pressure.

Synthesis Technique	**Si/Al**	**Mo loading** (wt %)	**Reaction Conditions** T (K)	P (kPa)	space velocity ($ml.gcat^{-1}.h^{-1}$)	**CH_4 conversion** (%)	**C_6H_6 selectivity** (%)	**Refs**
Incipient-wetness impregnation of aqueous $(NH_4)_6Mo_7O_{24}$• $4H_2O$	50	1	973	115	1500	1.4	82 [a]	118
		2				4.5	92.9 [a]	
		3				6.3	94.4 [a]	
		4.5				5.2	93.4 [a]	
		6				2.7	86.3 [a]	
		8				3.4	91.2 [a]	
		10				3.1	90 [a]	
Incipient-wetness impregnation of aqueous $(NH_4)_6Mo_7O_{24}$• $4H_2O$	23	1	973	-	1500	4.5	-	119
		2				6	-	
		4				12.5	-	
		8				9.5	-	
		10				8	-	
Wetness Impregnation of $(NH_4)_6Mo_7O_{24}$• $4H_2O$	20.4	-	973	101	3600	8	65	122
Wetness Impregnation combined with treatment by rotavapor		-				10.5	70	
Wetness Impregnation assisted by ultrasound treatment		-				11	70	
Wetness Impregnation assisted by		-				14.5	77	

microwave treatment								
Mechanical mixing of ZSM-5 with ammonium molybdate		-				7	62	
Impregnation of ammonium paramolybdate	25	2	1023	101	800 [d]	7.6	78.4	[9]
						7.9 [e]	72.2	
Solid state ion exchange of $MoCl_3$ with ZSM-5						2.6	71.5	
						7.5 [e]	71.2	
Incipient-wetness impregnation of aqueous $(NH_4)_6Mo_7O_{24}$	23	5	973	-	1500	12.5	38	[120]
Solvothermal synthesis						13	46	
Solvothermal synthesis utilizing 10 v% ethanol/water as solvent						15	33	
Impregnation of $(NH_4)_6Mo_7O_{24}$•$4H_2O$	25	2	973	200	1440	7.2	100	[8]
	50					4.4	100	
Physical mixing of MoO_3 and ZSM-5	15	2	1023	-	1500	18 [c]	67 [b]	[123]
	25					22 [c]	30 [b]	
	40					22 [c]	32 [b]	
Incipient wetness impregnation of $(NH_4)_6Mo_7O_{24}$•$4H_2O$	15	3	973	-	1550	8 [c]	70	[121]
	25					6 [c]	60	
	40					3 [c]	45	
Incipient-wetness impregnation of aqueous	17	2	993	-	1350	14 [c]	78	[124]

$(NH_4)_6Mo_7O_{24}$• $4H_2O$								
Wetness Impregnation of $(NH_4)_6Mo_7O_{24}$• $4H_2O$	13	2	973	20	15000 [d]	24.7 [f]	11.1	[107]
				50		27.8 [f]	18.5	
				100		34.0 [f]	26.1	
				200		48.0 [f]	31.4	
				300		63.3 [f]	34.2	
				400		84.5 [f]	39.2	
				600		103. 0 [f]	40.0	
				800		127.2 [f]	41.8	
				1000		137.2 [f]	41.3	
				1500		162.0 [f]	43.4	

[a] *Selectivity of all aromatic products are reported.*

[b] *C_6H_6 selectivity was back calculated from the knowledge of CH_4 conversion and C_6H_6 yield.*

[c] *CH_4 conversion was taken at the maximum C_6H_6 selectivity.*

[d] *Gas hourly space velocity: GHSV (h^{-1})*

[e] *pretreated with CO at 500 °C for 6 hours.*

[f] *CH_4 conversion is given as mmol/gcat. Average values were used for reproducible experiments.*

6. Kinetics and reaction mechanism of MDA over supported MO_x/ZSM-5 catalysts:

Rate-determining-step (RDS). The energy associated with the breaking of the C-H bond in the methane molecule (~437±2 kJ/mol)[3,125,126] is extremely high. Such a large energetic barrier requires high temperatures to initiate C-H bond activation, especially for the non-oxidative conversion of methane. The C-H bond breaking of CH_4 is, therefore, generally considered the rate-determining-step in methane chemical reactions.[56] Temperature programmed MDA studies with the CH_4 and CD_4 isotopes demonstrated a significant kinetic isotope effect (T_p=890 K for CH_4 and T_p=1042 K for CD_4) establishing that breaking of the C-H bond of methane is indeed the rate-determining-step.[56]

Most abundant reaction intermediate (MARI). Given that the RDS is the activation of the C-H bond upon adsorption of CH_4, all subsequent reaction steps will be extremely fast. This is confirmed by the immediate production of benzene and hydrogen over an activated catalyst (i.e., when the induction period is over). Consequently, the population of surface reaction intermediates will be negligible under MDA reaction conditions and difficult to detect spectroscopically. Gas-phase methyl radicals are also generated and their contribution to the MDA reaction must be quantified, but no such reports have appeared to date.[39]

Many studies have proposed ethylene and acetylene as the primary reaction intermediates for the MDA reaction.[39,127] One of the reasons cited for identifying ethylene and acetylene as reaction intermediates is that benzene is formed upon dosing either of these C_2 hydrocarbons over supported MO_x/ZSM-5 catalysts. The feeding of ethylene generally produces higher selectivity for toluene, whereas acetylene (as a feed) results in similar selectivity towards toluene and benzene, compared to that of methane. Moreover, the more reactive acetylene molecule exhibited higher benzene formation rates than ethylene.[99,108,112] It was also shown that acetylene was not observed as a side-product of the MDA reaction, possibly due to its high reactivity. Acetylene easily hydrogenates to ethylene in the presence of hydrogen, which may explain why some authors observed ethylene during MDA while a few observed acetylene.[128] To circumvent the gas-phase reactions of the acetylene intermediate, recently, low residence times in conjunction with microwave heating instead of conventional (resistive) heating, were used to establish a gas-solid temperature gradient provided by the selective heating and the low gas-solid contact time.[129] This approach apparently quenched gas-phase reactions and enabled detection of the acetylene and carbon monoxide intermediates in appreciable quantities. Over the same catalyst, acetylene was not detected using conventional heating reactor.[129] On the other hand, a recent report has cast

doubt on ethylene being the primary intermediate.[127] It was concluded that ethylene was *not* the major reaction intermediate because the hydrocarbon pool formed in the zeolite matrix during MDA is comprised of less dense and more hydrogenated species than the pool formed from ethylene.[127] Moreover, the carbonaceous deposits formed from methane were also more reactive than the ones formed from ethylene.[127] As mentioned above, the RDS is the cleavage of the C-H bond of CH_4 and, consequently, it is highly unlikely that reaction intermediates can be detected via conventional approaches because all steps after the RDS are expected to be extremely fast (especially at/above 973 K).

MDA reaction mechanism. The exact MDA mechanism remains under debate. Literature reports corroborating opposing proposals are available: (1) mono-functional mechanism with Mo sites being solely responsible for all catalytic steps, [99,112] and (2) bi-functional mechanism where Mo sites activate CH_4 and adjacent framework Brønsted acid sites polymerize and aromatize the C_2 intermediates. [130–132] The majority of MDA studies with supported Mo/ZSM-5, the most investigated MDA catalyst, reported that the Mo-carbide sites within the pores were responsible for the activation of C-H bond in methane and converting the CH_x intermediates into ethylene/acetylene. Subsequently, the ethylene/acetylene oligomerization and aromatization to benzene and other aromatic products was proposed to occur on the framework Brønsted acid sites in the zeolite micropores.[130–132] Alternatively, the mono-functional mechanism[99,107,112] proposes that both the activation of methane and subsequent reaction of the hydrocarbon pool to benzene exclusively occurs at Mo carbide sites.[127,133,134] It was recently reported that the supported Mo_xC_y/silicalite-1 catalyst, which doesn't contain Brønsted acidity and has the same topology as ZSM-5, was able to convert methane into benzene and aromatic coke at 973 K. It was, therefore, inferred that framework Brønsted acid sites were not *required* for MDA and that the conversion

of methane to benzene followed a mono-functional mechanism on highly dispersed Mo carbide species embedded in the 10MR zeolite micropores.[112] The lower catalytic performance of Mo_xC_y/silicalite-1 catalyst compared to the Mo/ZSM-5 catalyst was attributed to the lack of Brønsted acid sites that aid in stabilizing and dispersing both the initial MoO_x and Mo_xC_y active sites inside the zeolite pores. The presence of the hydrocarbon pool and hydrocarbon pool mechanism was experimentally verified by pulsing isotopically labelled CH_4 ($^{13}CH_4$, CD_4).[99,111] A recent computational study also determined that, at least over Mo_xC_y sites, the radical hydrocarbon-pool pathway was energetically less demanding and, thus, more favorable.[135] Currently, the exact mechanism of how the radical hydrocarbon-pool forms and cooperates during MDA to form benzene is not understood and requires further probing using *operando* spectroscopy studies with high spatial and temporal resolution.[108]

7. MoO_x/ZSM-5 Catalyst's Stability and Deactivation under MDA.

It is well known that ZSM-5 supported MDA catalysts experience systematic deactivation with time on stream due to coke formation leading to pore blockage, and due to larger MoO_x clusters at the external surface sintering at elevated temperature during reaction. Previously, process-intensification strategies have been proposed to circumvent the catalyst deactivation, which include cycling H_2 feed after CH_4 to reactivate the catalyst,[120] increasing the reaction pressure to 15 bar to speed up hydrogenation of deposited coke,[107] O_2-treatment to reverse both the carbide formation and the agglomeration of Mo nanostructures to regenerate the deactivated catalyst[42], and using low temperature H_2-pre-reduction before carburization to form a higher population of dispersed Mo_xC_y species.[136] The state-of-the art understanding regarding coking of Mo/ZSM-5 catalysts during reaction is that graphite-like external coke is more detrimental to the activity of

the catalyst than internal coke.[135] External coke formation leads to blockage of the pore openings, which in turn decreases the access of CH_4 to the zeolite channels.[135]

A noteworthy synthesis approach, aimed at improving Mo/ZSM-5 catalyst's stability, utilizes continuous solvothermal synthesis method under supercritical conditions and reducing atmosphere to synthesize 5% Mo/ZSM-5.[120] Although lacking *in-situ* or *operando* characterization of their material, the study boasts an impressive stable performance of the catalyst for ~15 hours on stream. The authors attributed enhanced stability of the catalyst prepared via the novel synthesis route to delayed formation of detrimental so-called hard coke species.[120] Very recently, however, 0.5%Mo was successfully loaded onto nano ZSM-5 to yield a single site Mo/ZSM-5 catalyst in contrast to a mixture of Mo phases typically present in traditionally prepared Mo/ZSM-5 catalysts.[137] This novel nano Mo/ZSM-5 material was shown be to orders of magnitude more stable than regular Mo/ZSM-5 catalysts, with the longest time on stream of 36 hours (3 cycles x 12 hours each), without an appreciable decrease in CH_4 conversion.[137] However, minor dealumination occurred in the material during multiple cycles, as evidenced by a decrease in unit cell volume.[137] Note that the degree of dealumination observed in this nano Mo/ZSM-5 catalyst was minuscule compared to that observed in traditionally prepared 1% Mo/ZSM-5 catalyst. It suffices to say that while this ultra-stable nano Mo/ZSM-5 synthesis approach has significantly improved the catalyst stability, various other synthetic approaches to impart greater stability found in zeolite-synthesis literature include encapsulation of metal ions/atoms during zeolite crystallization,[138] alkali-stabilized metal incorporation into zeolite pores,[139] stabilization of extra framework sites via substituted framework atoms to exploit strong-metal-support-interaction (SMSI) phenomena,[140–142] etc. An excellent, state-of-the-art review of the various strategies to improve zeolite-based catalysts' stability

towards prolonged operation under harsh reaction conditions, similar to those required for MDA, can be found elsewhere in the literature.[143]

8. Summary and Outlook:

There are still disagreements in the literature of MDA catalysis of supported MO_x/ZSM-5 catalysts primarily because of information gaps, despite a large number of publications on the topic. While the nature of the dispersed MO_x sites is much better understood for the group VI metal oxides in supported MO_x/ZSM-5 catalysts (Cr, Mo, W), more research is still needed for the ZSM-5 supported group V (V)-, group VII (Re)- and group VIII (Fe)-containing catalysts. Under MDA reaction conditions, the initially dispersed, fully oxidized MO_x sites become reduced to oxycarbide and carbide clusters that represent the catalytic active sites. The surface ReO_x site becomes reduced to metallic Re^0. The rds is the breaking of the C-H bond during the CH_4 adsorption step, which makes all subsequent steps kinetically insignificant. In terms of catalytic MDA performance, the supported MoO_x/ZSM-5 catalyst system appears to be the best candidate amongst all of the group V-VIII metal oxides discussed herein. With regards to the reaction mechanism, the literature leans towards the radical hydrocarbon pool mechanism proceeding with activation and aromatization at mono-functional metal carbide cluster sites. Considerable research on supported MO_x/ZSM-5 catalysts for MDA is expected in the coming years to address both the unresolved fundamental issues (molecular structures of the dehydrated surface MO_x sites, anchoring sites of the surface MO_x sites on the ZSM-5 support, and nature of catalytic active sites under MDA reaction conditions) and applied aspects (increasing benzene yield and deactivation from coking).

Further advancement of the fundamental structure-activity relationships of the MDA catalytic reaction using group V-VIII MO_x-based ZSM-5 catalysts to guide the rational design and optimization of these catalysts for MDA will require the following:

- Isotopic $^{18}O_2$-$^{16}O_2$ exchange *in-situ* Raman studies to determine the number of terminal M=O oxo bonds present for all the dehydrated surface MO_x sites on the ZSM-5 support.
- *Operando* Raman and XAS spectroscopy studies to completely understand the molecular structures of the catalytic active sites under the MDA reaction conditions.
- Complementary *operando* Near Atmospheric Pressure (NAP)-XPS, UV-vis DRS, and XAS studies to provide information about the oxidation states of the catalytic active sites during MDA.
- Modulation excitation spectroscopy (MES) and isotope-switch experiments to elucidate the nature of the reaction intermediates and reaction network.
- *Operando* photoelectron photoion coincidence spectroscopy (PEPICO)[144] and online synchrotron vacuum ultraviolet photoionization mass spectroscopy (SVUV-PIMS)[145] to provide information on the involvement of gas-phase radical species in the MDA mechanism.
- *Operando* UV-Vis analysis of carefully synthesized, oriented ZSM-5-based catalysts have recently shown the ability to unravel structure-function relationships by elucidating chemistries occurring within the zeolite pores versus the external surface.[146]

9. Conflicts of Interest:

There are no conflicts to declare.

10. Acknowledgements:

This work was supported by NSF CBET Award #1706581. All authors have read and agreed to the final version of the manuscript.

11. Author information

Daniyal Kiani: 0000-0002-9748-3007

Sagar Sourav: 0000-0001-5892-1329

Jonas Baltrusaitis: 0000-0001-5634-955X

Israel. E. Wachs: 0000-0001-5282-128X

References

1 T. Mokrani and M. Scurrell, *Catalysis Reviews*, 2009, **51**, 1–145.

2 M. B. Park, E. D. Park and W.-S. Ahn, *Frontiers in Chemistry*, 2019, **7**, 514.

3 D. Kiani, S. Sourav, J. Baltrusaitis and I. E. Wachs, *ACS Catalysis*, 2019, **9**, 5912–5928.

4 D. Kiani, S. Sourav, W. Taifan, M. Calatayud, F. Tielens, I. E. Wachs, J. Baltrusaitis, I. E. Wachs and J. Baltrusaitis, *ACS Catalysis*, 2020, **10**, 4580–4592.

5 D. Kiani, S. Sourav, I. E. Wachs and J. Baltrusaitis, *Catalysis Science & Technology*, 2020, **10**, 3334–3345.

6 Y. Gao, L. Neal, D. Ding, W. Wu, C. Baroi, A. M. Gaffney and F. Li, *ACS Catalysis*, 2019, **9**, 8592–8621.

7 B. M. Weckhuysen, D. Wang, M. P. Rosynek and J. H. Lunsford, *Journal of Catalysis*, 1998, **175**, 347–351.

8 L. Wang, L. Tao, M. Xie, G. Xu, J. Huang and Y. Xu, *Catalysis Letters*, 1993, **21**, 35–41.

9 B. M. Weckhuysen, D. Wang, M. P. Rosynek and J. H. Lunsford, *Journal of Catalysis*, 1998, **175**, 338–346.

10 J. Hao, P. Schwach, G. Fang, X. Guo, H. Zhang, H. Shen, X. Huang, D. Eggart, X. Pan and X. Bao, *ACS Catalysis*, 2019, **9**, 9045–9050.

11 M. Sakbodin, Y. Wu, S. C. Oh, E. D. Wachsman and D. Liu, *Angewandte Chemie - International Edition*, 2016, **55**, 16149–16152.

12 M. Moser, L. Rodríguez-García, A. P. Amrute and J. Pérez-Ramírez, *ChemCatChem*, 2013, **5**, 3520–3523.

13 V. Paunović, G. Zichittella, M. Moser, A. P. Amrute and J. Pérez-Ramírez, *Nature Chemistry*, 2016, **8**, 803–809.

14 G. Zichittella, V. Paunović, A. P. Amrute and J. Pérez-Ramírez, *ACS Catalysis*, 2017, **7**, 1805–1817.

15 J. Tollefson, “Flaring” wastes 3.5% of world’s natural gas.

16 Zero Routine Flaring by 2030, https://www.worldbank.org/en/programs/zero-routine-flaring-by-2030#1.

17 M. Wark, A. Brückner, T. Liese and W. Grünert, *Journal of Catalysis*, 1998, **175**, 48–61.

18 Y. F. Chang, G. A. Somorjai and H. Heinemann, *Journal of Catalysis*, 1995, **154**, 24–32.

19 A. de Lucas, J. L. Valverde, L. Rodriguez, P. Sanchez and M. T. Garcia, *Applied Catalysis A: General*, 2000, **203**, 81–90.

20 T. K. Katranas, K. S. Triantafyllidis, A. G. Vlessidis and N. P. Evmiridis, in *Oxide Based Materials*, eds. A. Gamba, C. Colella and S. B. T.-S. in S. S. and C. Coluccia, Elsevier, 2005, vol. 155, pp. 347–354.

21 P. K. Chaudhari, P. K. Saini and S. Chand, *Journal of Scientific and Industrial Research*, 2002, **61**, 810–816.

22 A. Z. Abdullah, M. Z. A. Bakar and S. Bhatia, *Catalysis Communications*, 2003, **4**, 555–560.

23 A. Z. Abdullah, M. Z. Abu Bakar and S. Bhatia, *Industrial & Engineering Chemistry Research*, 2003, **42**, 6059–6067.

24 H. S. Lacheen, P. J. Cordeiro and E. Iglesia, *Chemistry - A European Journal*, 2007, **13**, 3048–3057.

25 Y. Traa, B. Burger and J. Weitkamp, *Microporous and Mesoporous Materials*, 1999, **30**, 3–41.

26 N. Mimura, I. Takahara, M. Inaba, M. Okamoto and K. Murata, *Catalysis Communications*, 2002, **3**, 257–262.

27 H. Yamashita, S. Ohshiro, K. Kida, K. Yoshizawa and M. Anpo, *Research on Chemical Intermediates*, 2003, **29**, 881–890.

28 M. E. Swanson, H. L. Greene and S. Qutubuddin, *Applied Catalysis B: Environmental*, 2004, **52**, 91–108.

29 F. Solymosi and P. Tolmacsov, *Catalysis Letters*, 2004, **93**, 7–11.

30 N. A. S. Amin and S. E. Pheng, *Catalysis Communications*, 2006, **7**, 403–407.

31 W. Ding, G. D. Meitzner, D. O. Marler and E. Iglesia, *The Journal of Physical Chemistry B*, 2001, **105**, 3928–3936.

32 J. A. Biscardi, G. D. Meitzner and E. Iglesia, *Journal of Catalysis*, 1998, **179**, 192–202.

33 Y. Xu, M. Chen, T. Wang, B. Liu, F. Jiang and X. Liu, *Journal of Catalysis*, 2020, **387**, 102–118.

34 Y. Xu, M. Chen, B. Liu, F. Jiang and X. Liu, *Chemical Communications*, 2020, **56**, 4396–4399.

35 O. v Bragin, T. v Vasina, A. v Preobrazhenskii and Kh. M. Minachev, *Bulletin of the Academy of Sciences of the USSR, Division of chemical science*, 1989, **38**, 680.

36 O. v Bragin, T. v Vasina, Ya. I. Isakov, B. K. Nefedov, A. v Preobrazhenskii, N. v Palishkina and Kh. M. Minachev, *Bulletin of the Academy of Sciences of the USSR, Division of chemical science*, 1982, **31**, 847.

37 O. v Bragin, A. v Preobrazhenskii and A. L. Liberman, *Bulletin of the Academy of Sciences of the USSR, Division of chemical science*, 1974, **23**, 1599.

38 K. Sun, D. M. Ginosar, T. He, Y. Zhang, M. Fan and R. Chen, *Industrial & Engineering Chemistry Research*, 2018, **57**, 1768–1789.

39 I. Vollmer, I. Yarulina, F. Kapteijn and J. Gascon, *ChemCatChem*, 2019, **11**, 39–52.

40 J. J. Spivey and G. Hutchings, *Chemical Society Reviews*, 2014, **43**, 792–803.

41 S. Ma, X. Guo, L. Zhao, S. Scott and X. Bao, *Journal of Energy Chemistry*, 2013, **22**, 1–20.

42 J. Gao, Y. Zheng, J. M. Jehng, Y. Tang, I. E. Wachs and S. G. Podkolzin, *Science*, 2015, **348**, 686–690.

43 I. Julian, J. L. Hueso, N. Lara, A. Solé-Daurá, J. M. Poblet, S. G. Mitchell, R. Mallada and J. Santamaría, *Catalysis Science & Technology*, 2019, **9**, 5927–5942.

44 R. W. Borry, Y. H. Kim, A. Huffsmith, J. A. Reimer and E. Iglesia, *The Journal of Physical Chemistry B*, 1999, **103**, 5787–5796.

45 W. Li, G. D. Meitzner, R. W. Borry and E. Iglesia, *Journal of Catalysis*, 2000, **191**, 373–383.

46 H. S. Lacheen and E. Iglesia, *The Journal of Physical Chemistry B*, 2006, **110**, 5462–5472.

47 M. Petráš, B. Wichterlová, M. Petras and B. Wichterlova, *Journal of Physical Chemistry*, 1992, **96**, 1805–1809.

48 F. Ayari, M. Mhamdi, D. P. Debecker, E. M. Gaigneaux, J. Alvarez-Rodriguez, A. Guerrero-Ruiz, G. Delahay and A. Ghorbel, *Journal of Molecular Catalysis A: Chemical*, 2011, **339**, 8–16.

49 J. Gao, Y. Zheng, Y. Tang, J. M. Jehng, R. Grybos, J. Handzlik, I. E. Wachs and S. G. Podkolzin, *ACS Catalysis*, 2015, **5**, 3078–3092.

50 H. Liu, W. Shen, X. Bao and Y. Xu, *Journal of Molecular Catalysis A: Chemical*, 2006, **244**, 229–236.

51 I. Vollmer, G. Li, I. Yarulina, N. Kosinov, E. J. Hensen, K. Houben, D. Mance, M. Baldus, J. Gascon and F. Kapteijn, *Catalysis Science & Technology*, 2018, **8**, 916–922.

52 W. Liu and Y. Xu, *Journal of Catalysis*, 1999, **185**, 386–392.

53 D. Wang, J. H. Lunsford and M. P. Rosynek, *Journal of Catalysis*, 1997, **169**, 347–358.

54 R. G. Bell, R. A. Jackson and C. R. A. Catlow, *Zeolites*, 1992, **12**, 870–871.

55 V. Pashkova, P. Klein, J. Dedecek, V. Tokarová and B. Wichterlová, *Microporous and Mesoporous Materials*, 2015, **202**, 138–146.

56 Y. Zheng, Y. Tang, J. R. Gallagher, J. Gao, T. Miller, I. E. Wachs and S. G. Podkolzin, *Journal of Physical Chemistry C*, 2019, **123**, 22281–22292.

57 M. Agote-Arán, A. B. Kroner, H. U. Islam, W. A. Sławiński, D. S. Wragg, I. Lezcano-González and A. M. Beale, *ChemCatChem*, 2019, **11**, 473–480.

58 Z.-T. Xiong, H.-B. Zhang, G.-D. Lin and J.-L. Zeng, *Catalysis Letters*, 2001, **74**, 233–239.

59 H. S. Lacheen, P. J. Cordeiro and E. Iglesia, *Journal of the American Chemical Society*, 2006, **128**, 15082–15083.

60 Y. Wu, S. Holdren, Y. Zhang, S. C. Oh, D. T. Tran, L. Emdadi, Z. Lu, M. Wang, T. J. Woehl, M. Zachariah, Y. Lei and D. Liu, *Journal of Catalysis*, 2019, **372**, 128–141.

61 M. A. Vuurman and I. E. Wachs, *Journal of Physical Chemistry*, 1992, **96**, 5008–5016.

62 M. A. Vuurman, D. J. Stufkens, A. Oskam and I. E. Wachs, *Journal of Molecular Catalysis*, 1992, **76**, 263–285.

63 S. Lwin, C. Keturakis, J. Handzlik, P. Sautet, Y. Li, A. I. Frenkel, I. E. Wachs, A. I. Frenkel, I. E. Wachs, A. I. Frenkel and I. E. Wachs, *ACS Catalysis*, 2015, **5**, 1432–1444.

64 S. Lwin, Y. Li, A. I. Frenkel and I. E. Wachs, *ACS Catalysis*, 2015, **5**, 6807–6814.

65 H.-Y. Chen and W. M. H. Sachtler, *Catalysis Today*, 1998, **42**, 73–83.

66 P. Marturano, L. Drozdová, A. Kogelbauer and R. Prins, *Journal of Catalysis*, 2000, **192**, 236–247.

67 G. Wu, F. Hei, N. Zhang, N. Guan, L. Li and W. Grünert, *Applied Catalysis A: General*, 2013, **468**, 230–239.

68 M. P. McDaniel, eds. D. D. Eley, H. Pines and P. B. B. T.-A. in C. Weisz, Academic Press, 1985, vol. 33, pp. 47–98.

69 C. Moisii, E. W. Deguns, A. Lita, S. D. Callahan, L. J. van de Burgt, D. Magana and A. E. Stiegman, *Chemistry of Materials*, 2006, **18**, 3965–3975.

70 B. M. Weckhuysen and I. E. Wachs, *The Journal of Physical Chemistry B*, 1997, **101**, 2793–2796.

71 D. K. Pappas, K. Kvande, M. Kalyva, M. Dyballa, K. A. Lomachenko, B. Arstad, E. Borfecchia, S. Bordiga, U. Olsbye, P. Beato and S. Svelle, *Catalysis Today*, DOI:https://doi.org/10.1016/j.cattod.2020.06.050.

72 K. Yoshizawa and Y. Shiota, *Journal of the American Chemical Society*, 2006, **128**, 9873–9881.

73 M. A. Newton, A. J. Knorpp, V. L. Sushkevich, D. Palagin and J. A. van Bokhoven, *Chemical Society Reviews*, 2020, **49**, 1449–1486.

74 A. v. Kucherov and A. A. Slinkin, *Journal of Molecular Catalysis*, 1994, **90**, 323–354.

75 A. V. Kucherov and A. A. Slinkin, *Zeolites*, 1987, **7**, 38–42.

76 E. Gillis and E. Boesman, *physica status solidi (b)*, 1966, **14**, 337–347.

77 C. Moisii, L. J. van de Burgt and A. E. Stiegman, *Chemistry of Materials*, 2008, **20**, 3927–3935.

78 E. L. Lee, I. E. Wachs, E. L. Lee and I. E. Wachs, *The Journal of Physical Chemistry C*, 2007, **111**, 14410–14425.

79 X. Gao, S. R. Bare, B. M. Weckhuysen, I. E. Wachs, *The Journal of Physical Chemistry B*, 1998, **102**, 10842–10852.

80 K. Nakamoto, *Infrared and Raman Spectra of Inorganic and Coordination Compounds,* John Wiley & Sons, Ltd, 6th edn., 1988, vol. 92.

81 T. Tanaka, H. Yamashita, R. Tsuchitani, T. Funabiki and S. Yoshida, *J. Chem. Soc., Faraday Trans. 1*, 1988, **84**, 2987–2999.

82 E. L. Lee and I. E. Wachs, in *Silica and Silicates in Modern Catalysis*, 2010, pp. 375–404.

83 X. Gao and I. E. Wachs, *The Journal of Physical Chemistry B*, 2000, **104**, 1261–1268.

84 Y. Tang, 2014. "Nature of Catalytic Active Sites in Supported MOx/ZSM-5 Catalysts: Anchoring Sites, Electronic Structures, Molecular Structures and Reactivity" (2014). *Theses and Dissertations*. 2835. https://preserve.lehigh.edu/etd/2835

85 C. A. Carrero, R. Schloegl, I. E. Wachs, R. Schomaecker, *ACS Catalysis*, 2014, **4**, 3357–3380.

86 N. R. Jaegers, C. Wan, M. Y. Hu, M. Vasiliu, D. A. Dixon, E. Walter, I. E. Wachs, Y. Wang, J. Z. Hu, *Journal of Physical Chemistry C*, 2017, **121**, 6246–6254.

87 B. Wichterlová, Z. Tvarůžková and J. Nováková, *Journal of the Chemical Society, Faraday Transactions 1: Physical Chemistry in Condensed Phases*, 1983, **79**, 1573–1583.

88 N. Mimura, M. Okamoto, H. Yamashita, S. Ted Oyama and K. Murata, *The Journal of Physical Chemistry B*, 2006, **110**, 21764–21770.

89 R. Rachapudi, P. S. Chintawar and H. L. Greene, *Journal of Catalysis*, 1999, **185**, 58–72.

90 A. Müller, K. H. Schmidt, E. Ahlborn and C. J. L. Lock, *Spectrochimica Acta Part A: Molecular Spectroscopy*, 1973, **29**, 1773–1788.

91 E. L. Lee and I. E. Wachs, *The Journal of Physical Chemistry C*, 2008, **112**, 6487–6498.

92 Y. Yu, G. Xiong, C. Li and F.-S. Xiao, *Microporous and Mesoporous Materials*, 2001, **46**, 23–34.

93 P. K. Dutta and M. Puri, *The Journal of Physical Chemistry*, 2002, **91**, 4329–4333.

94 A. M. Rzhevskii, P. Choi, F. H. Ribeiro, R. J. Gulotty and M. M. Olken, *Catalysis Letters*, 2001, **73**, 187–191.

95 H. Tian, I. E. Wachs and L. E. Briand, *The Journal of Physical Chemistry B*, 2005, **109**, 23491–23499.

96 A. Chakrabarti and I. E. Wachs, *ACS Catalysis*, 2018, **8**, 949–959.

97 H. Tian, C. A. Roberts and I. E. Wachs, *The Journal of Physical Chemistry C*, 2010, **114**, 14110–14120.

98 I. Lezcano-González, R. Oord, M. Rovezzi, P. Glatzel, S. W. Botchway, B. M. Weckhuysen and A. M. Beale, *Angewandte Chemie International Edition*, 2016, **55**, 5215–5219.

99 N. Kosinov, A. S. G. Wijpkema, E. Uslamin, R. Rohling, F. J. A. G. Coumans, B. Mezari, A. Parastaev, A. S. Poryvaev, M. v. Fedin, E. A. Pidko and E. J. M. Hensen, *Angewandte Chemie*, 2018, **130**, 1028–1032.

100 E. I. Ross-Medgaarden and I. E. Wachs, *Journal of Physical Chemistry C*, 2007, **111**, 15089–15099.

101 E. I. Ross-Medgaarden, W. v. Knowles, T. Kim, M. S. Wong, W. Zhou, C. J. Kiely and I. E. Wachs, *Journal of Catalysis*, 2008, **256**, 108–125.

102 D. S. Kim, M. Ostromecki and I. E. Wachs, *Journal of Molecular Catalysis A: Chemical*, 1996, **106**, 93–102.

103 I. E. Wachs, T. Kim and E. I. Ross, *Catalysis Today*, 2006, **116**, 162–168.

104 D. Kiani, G. Belletti, P. Quaino, F. Tielens and J. Baltrusaitis, *The Journal of Physical Chemistry C*, 2018, **122**, 24190–24201.

105 H.-Y. Chen, E.-M. El-Malki, X. Wang, R. A. van Santen and W. M. H. Sachtler, *Journal of Molecular Catalysis A: Chemical*, 2000, **162**, 159–174.

106 I. Vollmer, S. Ould-Chikh, A. Aguilar-Tapia, G. Li, E. Pidko, J.-L. Hazemann, F. Kapteijn and J. Gascon, *Journal of the American Chemical Society*, 2019, **141**, 18814–18824.

107 N. Kosinov, E. A. Uslamin, L. Meng, A. Parastaev, Y. Liu and E. J. M. Hensen, *Angewandte Chemie - International Edition*, 2019, **58**, 7068–7072.

108 G. Li, I. Vollmer, C. Liu, J. Gascon and E. A. Pidko, *ACS Catalysis*, 2019, **9**, 8731–8737.

109 I. Vollmer, N. Kosinov, Á. Szécsényi, G. Li, I. Yarulina, E. Abou-Hamad, A. Gurinov, S. Ould-Chikh, A. Aguilar-Tapia, J.-L. Hazemann, E. Pidko, E. Hensen, F. Kapteijn and J. Gascon, *Journal of Catalysis*, 2019, **370**, 321–331.

110 I. Vollmer, B. van der Linden, S. Ould-Chikh, A. Aguilar-Tapia, I. Yarulina, E. Abou-Hamad, Y. G. Sneider, A. I. Olivos Suarez, J.-L. Hazemann, F. Kapteijn and J. Gascon, *Chemical Science*, 2018, **9**, 4801–4807.

111 N. Kosinov, E. A. Uslamin, F. J. A. G. Coumans, A. S. G. Wijpkema, R. Y. Rohling and E. J. M. Hensen, *ACS Catalysis*, 2018, **8**, 8459–8467.

112 N. Kosinov, F. J. A. G. Coumans, E. A. Uslamin, A. S. G. Wijpkema, B. Mezari and E. J. M. Hensen, *ACS Catalysis*, 2016, **7**, 520–529.

113 V. v Kozlov, V. I. Zaikovskii, A. v Vosmerikov, L. L. Korobitsyna and G. v Echevskii, *Kinetics and Catalysis*, 2008, **49**, 110–114.

114 C. J. Keturakis, M. Zhu, E. K. Gibson, M. Daturi, F. Tao, A. I. Frenkel and I. E. Wachs, *ACS Catalysis*, 2016, **6**, 4786–4798.

115 M. Zhu and I. E. Wachs, *ACS Catalysis*, 2016, **6**, 1764–1767.

116 M. Zhu and I. E. Wachs, *ACS Catalysis*, 2016, **6**, 722–732.

117 B. M. Weckhuysen, D. Wang, P. Michael and J. H. Lunsford, *Angewandte Chemie - International Edition*, 1997, **36**, 2374–2376.

118 Y. Xu, W. Liu, S.-T. Wong, L. Wang and X. Guo, *Catalysis Letters*, 1996, **40**, 207–214.

119 A. López-Martín, A. Caballero and G. Colón, *Molecular Catalysis*, 2020, **486**, 110787.

120 I. Julian, M. B. Roedern, J. L. Hueso, S. Irusta, A. K. Baden, R. Mallada, Z. Davis and J. Santamaria, *Applied Catalysis B: Environmental*, 2020, **263**, 118360.

121 M. Rahman, A. Infantes-Molina, A. S. Hoffman, S. R. Bare, K. L. Emerson and S. J. Khatib, *Fuel*, 2020, **278**, 118290.

122 K. Velebná, M. Horňáček, V. Jorík, P. Hudec, M. Čaplovičová and L. Čaplovič, *Microporous and Mesoporous Materials*, 2015, **212**, 146–155.

123 J.-P. Tessonnier, B. Louis, S. Rigolet, M. J. Ledoux and C. Pham-Huu, *Applied Catalysis A: General*, 2008, **336**, 79–88.

124 E. v Matus, I. Z. Ismagilov, O. B. Sukhova, V. I. Zaikovskii, L. T. Tsikoza, Z. R. Ismagilov and J. A. Moulijn, *Industrial & Engineering Chemistry Research*, 2007, **46**, 4063–4074.

125 D. Wolf, *Angewandte Chemie - International Edition*, 1999, **37**, 3351–3353.

126 P. Schwach, X. Pan and X. Bao, *Chemical Reviews*, 2017, **117**, 8497–8520.

127 I. Vollmer, E. Abou-Hamad, J. Gascon and F. Kapteijn, *ChemCatChem*, 2020, **12**, 544–549.

128 P. Tsai and J. R. Anderson, *Journal of Catalysis*, 1983, **80**, 207–214.

129 I. Julian, H. Ramirez, J. L. Hueso, R. Mallada and J. Santamaria, *Chemical Engineering Journal*, 2019, **377**, 119764.

130 K. S. Wong, J. W. Thybaut, E. Tangstad, M. W. Stöcker and G. B. Marin, *Microporous and Mesoporous Materials*, 2012, **164**, 302–312.

131 C. Karakaya, H. Zhu and R. J. Kee, *Chemical Engineering Science*, 2015, **123**, 474–486.

132 M. C. Iliuta, I. Iliuta, B. P. A. Grandjean and F. Larachi, *Industrial & Engineering Chemistry Research*, 2003, **42**, 3203–3209.

133 P. Mériaudeau, L. v. Tiep, V. T. T. T. Ha, C. Naccache and G. Szabo, *Journal of Molecular Catalysis A: Chemical*, 1999, **144**, 469–471.

134 P. Mériaudeau, V. T. T. Ha and L. van Tiep, *Catalysis Letters*, 2000, **64**, 49–51.

135 X. Huang, X. Jiao, M. Lin, K. Wang, L. Jia, B. Hou and D. Li, *Catalysis Science & Technology*, 2018, **8**, 5740–5749.

136 M. Rahman, A. Infantes-Molina, A. Boubnov, S. R. Bare, E. Stavitski, A. Sridhar and S. J. Khatib, *Journal of Catalysis*, 2019, **375**, 314–328.

137 S. v. Konnov, F. Dubray, E. B. Clatworthy, C. Kouvatas, J. P. Gilson, J. P. Dath, D. Minoux, C. Aquino, V. Valtchev, S. Moldovan, S. Koneti, N. Nesterenko and S. Mintova, *Angewandte Chemie*, , DOI:10.1002/ange.202006524.

138 L. Liu, U. Díaz, R. Arenal, G. Agostini, P. Concepción and A. Corma, *Nature Materials*, 2017, **16**, 132–138.

139 M. Yang, S. Li, Y. Wang, J. A. Herron, Y. Xu, L. F. Allard, S. Lee, J. Huang, M. Mavrikakis and M. Flytzani-Stephanopoulos, *Science*, 2014, **346**, 1498 LP – 1501.

140 Z. Xu, Y. Yue, X. Bao, Z. Xie and H. Zhu, *ACS Catalysis*, 2020, **10**, 818–828.

141 Y. Wang, Z.-P. Hu, W. Tian, L. Gao, Z. Wang and Z.-Y. Yuan, *Catalysis Science & Technology*, 2019, **9**, 6993–7002.

142 R. Ryoo, J. Kim, C. Jo, S. W. Han, J.-C. Kim, H. Park, J. Han, H. S. Shin and J. W. Shin, *Nature*, 2020, **585**, 221–224.

143 E. B. Clatworthy, S. v. Konnov, F. Dubray, N. Nesterenko, J. P. Gilson and S. Mintova, *Angewandte Chemie*, 2020, 2–21.

144 G. Zichittella, P. Hemberger, F. Holzmeier, A. Bodi and J. Pérez-Ramírez, *The Journal of Physical Chemistry Letters*, 2020, **11**, 856–863.

145 X. Zhang, R. You, Z. Wei, X. Jiang, J. Yang, Y. Pan, P. Wu, Q. Jia, Z. Bao, L. Bai, M. Jin, B. Sumpter, V. Fung, W. Huang and Z. Wu, *Angewandte Chemie International Edition*, , DOI:10.1002/anie.202002440.

146 D. Fu, O. van der Heijden, K. Stanciakova, J. E. Schmidt and B. M. Weckhuysen, *Angewandte Chemie International Edition*, , DOI:10.1002/anie.201916596.

Table of Contents Entry

The literature on methane dehydroaromatization (MDA) to benzene using ZSM-5 supported, group V-VIII transition metal-based catalysts (MO_x/ZSM-5) is critically reviewed with a focus on *in-situ* and *operando* molecular insights.